R-06-101

Simulation of hydrodynamic effects of salt rejection due to permafrost

Hydrogeological numerical model of density-driven mixing, at a regional scale, due to a high salinity pulse

Patrik Vidstrand, BERGAB

Urban Svensson, CFE AB

Sven Follin, SF GeoLogic

October 2006

Svensk Kärnbränslehantering AB
Swedish Nuclear Fuel
and Waste Management Co
Box 5864
SE-102 40 Stockholm Sweden
Tel 08-459 84 00
+46 8 459 84 00
Fax 08-661 57 19
+46 8 661 57 19

ISSN 1402-3091
SKB Rapport R-06-101

Simulation of hydrodynamic effects of salt rejection due to permafrost

Hydrogeological numerical model of density-driven mixing, at a regional scale, due to a high salinity pulse

Patrik Vidstrand, BERGAB

Urban Svensson, CFE AB

Sven Follin, SF GeoLogic

October 2006

Abstract

The main objective of this study is to support the safety assessment of the investigated candidate sites concerning hydrogeological and hydrogeochemical issues related to permafrost. However, a more specific objective of the study is to improve the assessment of processes in relation to permafrost scenarios.

The model is based on a mathematical model that includes Darcy velocities, mass conservation, matrix diffusion, and salinity distribution. Gravitational effects are thus fully accounted for. A regional groundwater flow model (POM v1.1, Simpevarp) was used as basis for the simulations.

The main results of the model include salinity distributions in time.

The general conclusion is that density-driven mixing processes are contained within more permeable deformation zones and that these processes are fast as compared with preliminary permafrost growth rates.

The results of the simulation suggest that a repository volume in the rock mass in-between the deterministic deformation zones, approximately 150 m below the permafrost will not experience a high salinity situation due to the salt rejection process.

Sammanfattning

Det huvudsakliga syftet med denna studie är att vara ett stöd för säkerhetsanalyser vid platsundersökningarna avseende hydrogeologisk och hydrogeokemiska påverkan från permafrost. Ett mer specifikt mål är att öka medvetandet om hydrogeologisk processhantering i permafrostscenarier.

Modellen är baserad på en matematisk modell som inkluderar Darcyhastigheter, masskonservering, matrisdiffusion och salinitetsfördelningar. Hänsyn har tagits till gravitationseffekter. En regional grundvattenmodell (POM v1.1, Simpevarp) ligger som grund för simuleringarna.

Det huvudsakliga resultatet av modellen inkluderar salinitetsfördelningar och deras tidsvariation.

Den allmänna slutsatsen är att densitetsdriven mixing sker i de mer permeabla deformationszonerna och att dessa mixingsprocesser är snabba i jämförelse med preliminära beräkningar av permafrostens tillväxthastighet.

Simuleringsresultaten indikerar att en förvarsvolym placerad utanför de deterministiska deformationszonerna, ungefär 150 meter under permafrosten inte kommer att utsättas för en hög salthalt på grund av utfrysning av salt under permafrost förhållanden.

Contents

1 Introduction

1.1 Background

In the necessary life-length of a deep repository for nuclear waste, climatic models predict future climatic situations that yield permafrost as well as glacial conditions. It is therefore stated that permafrost situations are viewed as one of the key surface climate domains that may exist in large parts of Scandinavia /SKB 2006/. Permafrost as surface boundary causes changes within the subsurface environment in hydrogeochemical as well as in hydrogeological properties. These changes in properties may result in a subsurface environment that affects the integrity of the barriers around a deep repository.

One possible change is due to the postulated salt rejection due to the freezing of groundwater in the subsurface permafrost regions. As reported in /Vidstrand 2003/ it is frequently assumed that a saline water stays as an unstable basal cryopeg just beneath the permafrost and only slowly mixes with the deeper groundwater. However, the occurrence of preferential flow-paths, such as in fractures and fracture zones, may trigger “fingering” and initiate a density-driven groundwater flow along with the additional mixing of groundwater types e.g. /Simmons et al. 2001/.

As background for the safety assessments for the candidate sites, Forsmark and Oskarshamn, this modelling study of the problem concerning increased salinity due to potential salt rejection during permafrost has been performed.

1.2 Scope and objectives

The main objective of this study is to support the safety assessment of the investigated candidate sites concerning hydrogeochemical issues related to permafrost. However, a more specific objective of the study is to improve the assessment of processes in relation to permafrost and increase the understanding of essential palaeohydrogeochemical as well as palaeohydrogeological situations.

1.3 Settings and limitations

The geometrical descriptions and present day boundary conditions for the model used are those of the hydrogeological model POM v1.1 adopted by a team working with the code DarcyTools v2.1 / Follin et al. 2004/. Therefore this study comprises the same limitations and sensitivities as this parent model.

The intention of this study is to assess conservative initial conditions of the permafrost processes. Since the knowledge of the actual conditions within the advancing permafrost is limited, the inputs on permafrost growth are based on numerical simulations that have used continuum and homogeneous porous medium descriptions. However, the physics of permafrost growth in fractured crystalline bedrock is not fully understood and the predictions of growth rate on a smaller scale may therefore be uncertain. The degree of conservatism in the initial conditions used in our palaeohydrogeological simulations is hence not possible to verify.

The study is restricted to advective-diffusive flow processes along with matrix diffusion.

The main driving force within the model is the density differences due to a saline water pulse initially released at the top boundary of the model. A temperature field is included with linear increase from zero degrees Centigrade at the permafrost interface.

1.4 Organisation of work and layout of report

The numerical modelling in this study was performed by a modelling team with expertise from BERGAB, Computer-aided Fluid Engineering (CFE), SF Geologic, and SKB. SF Geologic supplied the geometrical framework, BERGAB and CFE created the initial conditions, and BERGAB performed and analysed the simulations and wrote the report. The DarcyTools code is developed by CFE on behalf of SKB /Svensson et al. 2004, Svensson and Ferry 2004, Svensson 2004/.

This report presents a number of simulations of generic permafrost situations. These were performed to investigate the potential impact of salt rejection in the geosphere. Chapter 2 gives some essential information about the DarcyTools code used. Chapter 3 presents some results from generic 2D simulations performed to investigate the influence of different characteristics (properties) and boundary conditions on the model results. Chapter 4 presents the over-all model methodology, model specifications and deliverables. Chapter 5 present the results from the transient flow and salinity simulations, and Chapter 6 contains a discussion on the relevance and possibilities of the simulations and presents the conclusions drawn by the investigation.

2 Hydrogeological modelling with DarcyTools

The computer code DarcyTools is developed for simulations of groundwater flow and mass transport in porous and fractured media; the code uses continuum equations.

The porous media considered is the soil cover consisting of Quaternary deposits on top of the bedrock surface. The fractured media is a crystalline rock mass of sparse fracture intensity traversed by large scale hydraulic conductors consisting of fracture zones. Hence, DarcyTools is well suited for numerical groundwater flow simulations in accordance with SKB's systems approach /Rhén et al. 2003/.

DarcyTools incorporates a number of novel modelling features of which the methodology to generate grid properties from a network of discrete fractures is among the most fundamental. This methodology assesses geometrical and hydrogeological properties of every unique fracture directly in the computational grid. As a result this methodology is believed to results in very accurate anisotropy in properties along with a relevant connectivity pattern of fractured bedrock.

The basics of the fractured media is a geological model of the larger scale deformation zones along with the geological characteristics of the bedrock properties between these deformation zones. The larger scale deformation zones are incorporated as deterministic features whereas the fractures between these deformation zones are stochastically generated within the code based on known geological characteristics. Additional to the known characteristics a series of assumptions are made:

- Fracture orientation distribution is univariate Fisher.
- Fracture length (size) distribution is a power-law distribution (similar to Pareto).
- Fracture spatial model is a Poisson point process.
- A power-law relationship between fracture length and fracture transmissivity.

Within the DarcyTools code, generated fractures that are confined within a unique numerical cell is omitted through a sorting process. It has been shown that this sorting process creates a fracture spatial model that goes from a Poisson point process to a weak fractal process Appendix C in /Follin et al. 2006/.

The used assumptions have not been singularly proven. However, established site specific empirical relationships do in parts validate the assumptions used e.g. /Darcel 2003, Vidstrand 2004/.

The DarcyTools code is based on a finite volume formulation of the governing differential equations for flow and mass transport. This means that the hydraulic properties of the computational grid cells are volumetric functions of:

- The chosen grid resolution.
- Assigned characteristics and properties of large scale deformation zones.
- Assigned characteristics and properties of small scale fractures.
- Assigned characteristics and properties of "background" fractures (on a scale too small to be discretisased).

Detailed descriptions of the concepts, methods, and equations of DarcyTools are documented in /Svensson et al. 2004/.

3 Generic case simulations

The mixing of the high saline water beneath a permafrost layer resulting from advective flow, caused by density differences is studied. It is postulated that this process is affected by properties such as porosity and hydraulic conductivity of the bedrock, and geometrical descriptions of these properties along with the difference in salinity of the waters.

A series of different generic cases have been investigated in 2D; however some cases have been tested within idealised 3D models. The main characteristics of these cases have been:

- Homogeneous medium.
- Homogeneous medium traversed by fracture zones.
- Fractured medium traversed by fracture zones.

Regarding the source of the high salinity water different settings have been investigated using various salinity values of the source along with different numerical time steps.

- Constant point source of high salinity water.
- Constant linear source of high salinity water.
- Pulse of linear source of high salinity water.

The influence of a regional flow across the model domain has also been investigated.

The first set of figures illustrates the influence of salinity and hydraulic conductivity on the results; all simulations are 100 years long.

Figure 3-1a and Figure 3-1b illustrate how the mixing processes develop around one or more single release locations. This could be seen as single locations of some small difference in properties or salinity. The results presented in Figure 3-1c indicate the starting of mixing (a very weak instability response seen as small undulations in the colouring) for the case of higher hydraulic conductivity. This is interesting since the model is a perfect homogenous and isotropic model and the instability needed to trigger convection cells can therefore only come from small numerical round-off errors. Even if this is a numerical artefact, this will happen in

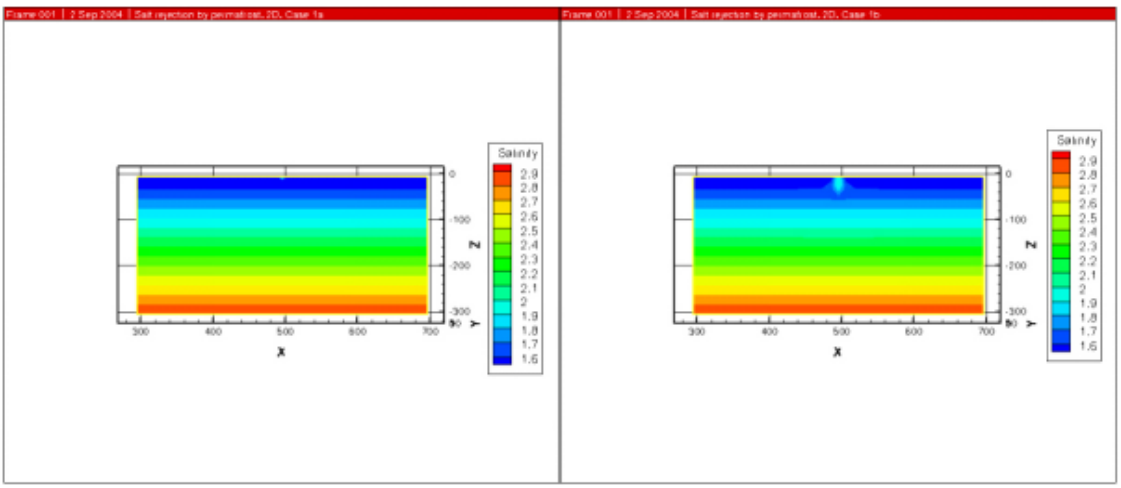

Figure 3-1a. *One point source of constant salinity of 2% released in a homogeneous medium. In the left illustration hydraulic conductivity equals $1.0 \cdot 10^{-7}$ [m/s] and in the right the Hydraulic conductivity value is 100 times larger. In the figures z=0 corresponds to the bottom of the permafrost, and not to ground surface.*

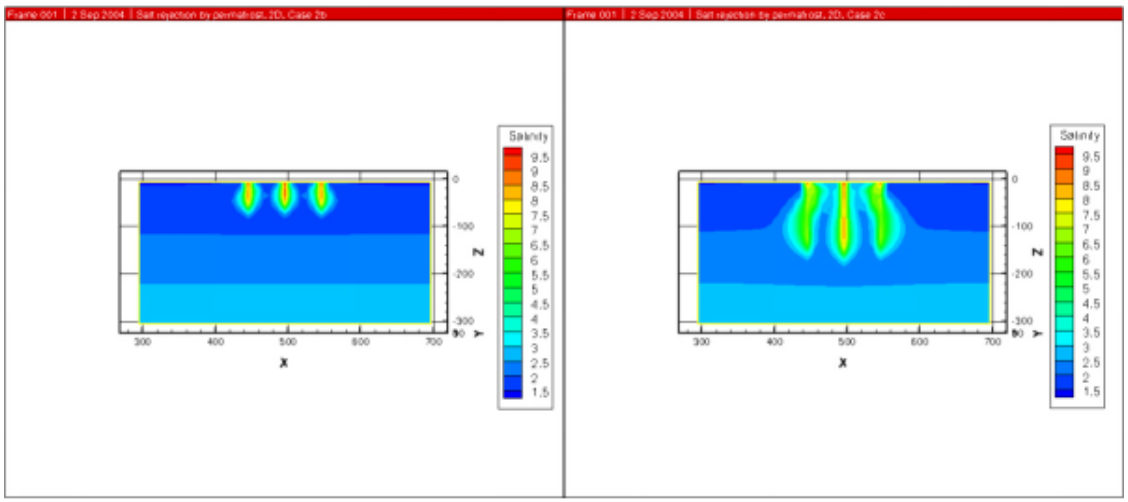

Figure 3-1b. *Three point sources of constant salinity of 10% released in a homogeneous medium. In the left illustration hydraulic conductivity equals $1.0 \cdot 10^{-6}$ [m/s] and in the right the Hydraulic conductivity value is 3 times larger. In the figures z=0 corresponds to the bottom of the permafrost, and not to ground surface.*

a "real world" situation since a perfect homogenous model does not exist. A small difference in salinity or hydraulic conductivity is all that is needed to trigger this mixing. In all simulations tested instabilities always occur at the boundaries while within the model domain the locations of instabilities seem to occur more by chance. All locations where the instability are introduced could be seen as a position with a small difference in hydraulic conductivity that initiates the mixing processes. In Figure 3-1d the salinity is increased to 40% compared to 10% in Figure 3-1c.

The results support the general assessment that both the salinity value and the bedrock hydraulic conductivity are important. The results further suggest that the hydraulic conductivity needs to be relatively high in order for significant mixing to occur. As a consequence it may be assumed that large fracture zones may control the mixing processes and that the matrix rock (of a typical Swedish site) will be relatively unaffected by these advective processes.

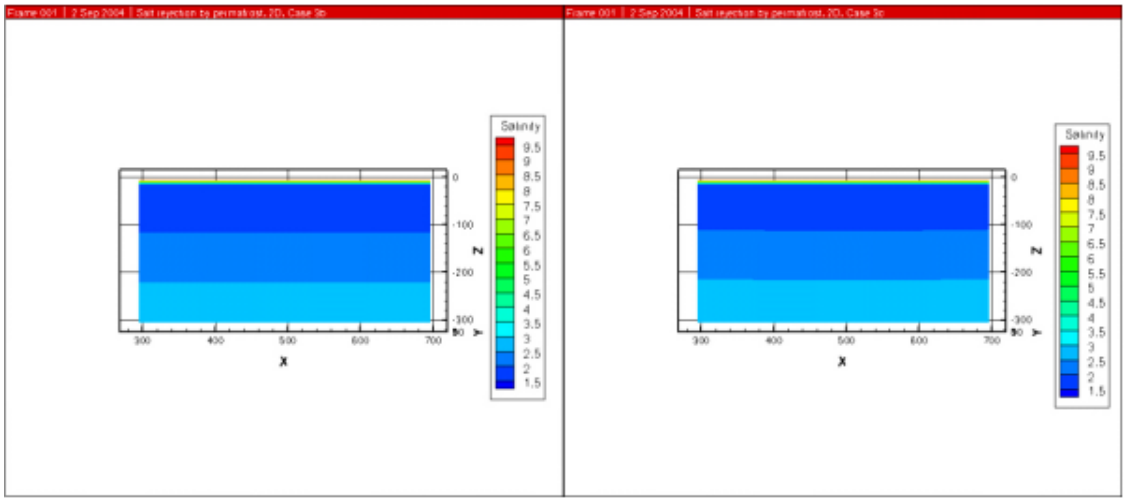

Figure 3-1c. *Linear sources of constant salinity of 10% released in a homogeneous medium. In the left illustration hydraulic conductivity equals $3.0 \cdot 10^{-6}$ [m/s] and in the right the Hydraulic conductivity value is $1.0 \cdot 10^{-5}$ [m/s]. In the figures z=0 corresponds to the bottom of the permafrost, and not to ground surface.*

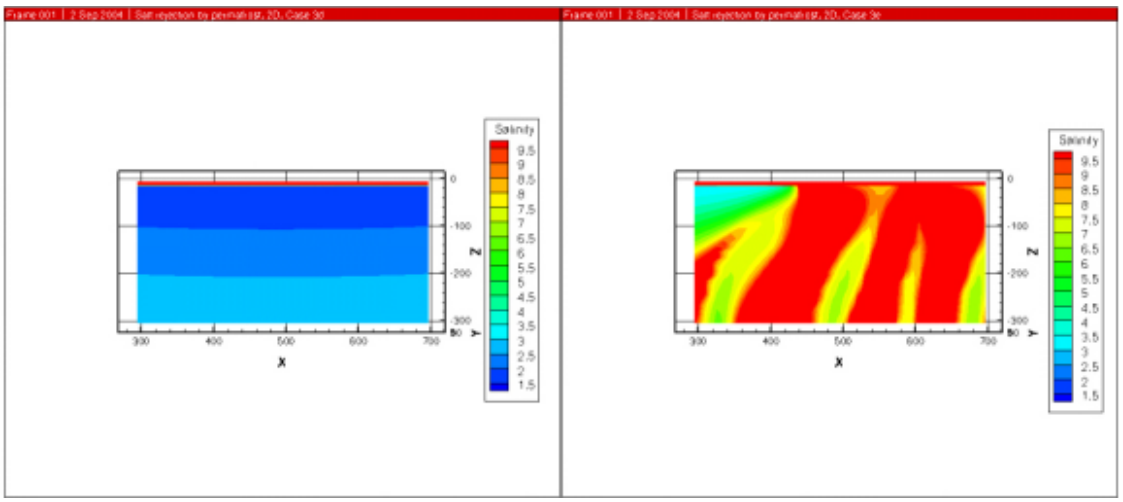

Figure 3-1d. *Linear sources of constant salinity of 40% released in a homogeneous medium. In the left illustration hydraulic conductivity equals $3.0 \cdot 10^{-6}$ [m/s] and in the right the Hydraulic conductivity value is $1.0 \cdot 10^{-5}$ [m/s]. In the figures z=0 corresponds to the bottom of the permafrost, and not to ground surface.*

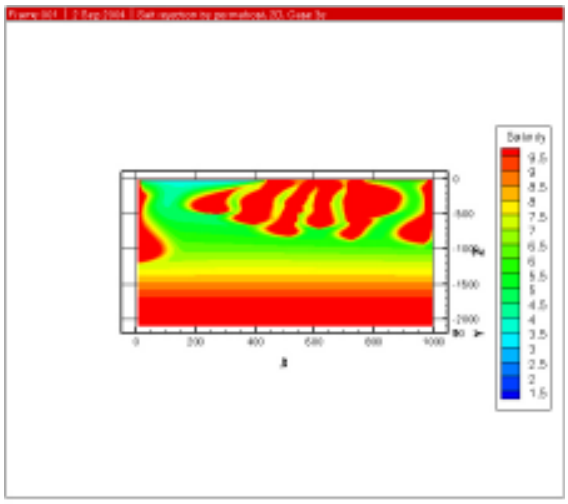

Figure 3-1e. *Linear sources of constant salinity of 40% all same as Figure 3-1d (right), entire model domain, situation after 100 years. In the figure z=0 corresponds to the bottom of the permafrost, and not to ground surface.*

It is assumed here that before permafrost occurs there is a gradual groundwater salinity profile, from diluted water of meteoric origin at the surface to highly saline water at depth. All modelling cases presented have an initial condition of salinity increasing linearly from 1.44% at the bottom of the permafrost to 10% at 2,100 m depth. For present day conditions, a salinity value of 1.44% corresponds to the expected groundwater salinity at a depth of 300 m before the onset of the permafrost. The surface boundary is in all cases a no-flow boundary caused by permafrost; initially a pulse of high salinity water (approximately 40% by weight of salt in the first cell layer, 10 m thick) is released all along this surface.

The first series of simulations investigate the influence of fracture zones within a homogeneous medium. In the right set of illustrations in Figure 3-2a–e, two vertical fracture zones are located at x = 300 [m] and x = 700 [m]. The hydraulic conductivity in the homogeneous medium is $1.0 \cdot 10^{-8}$ [m/s] and the porosity is $1.0 \cdot 10^{-5}$[–]. The hydraulic conductivity of the fracture zones is one order of magnitude larger.

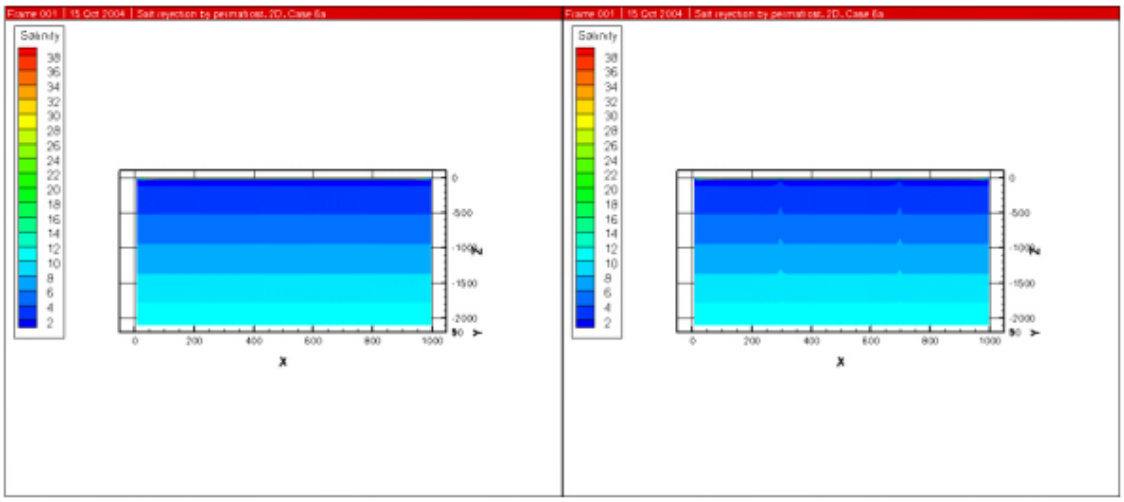

Figure 3-2a. *Salinity distribution after one month for (left) homogeneous model and (right) homogeneous model traversed by two vertical fracture zones. In the figures z=0 corresponds to the bottom of the permafrost, and not to ground surface.*

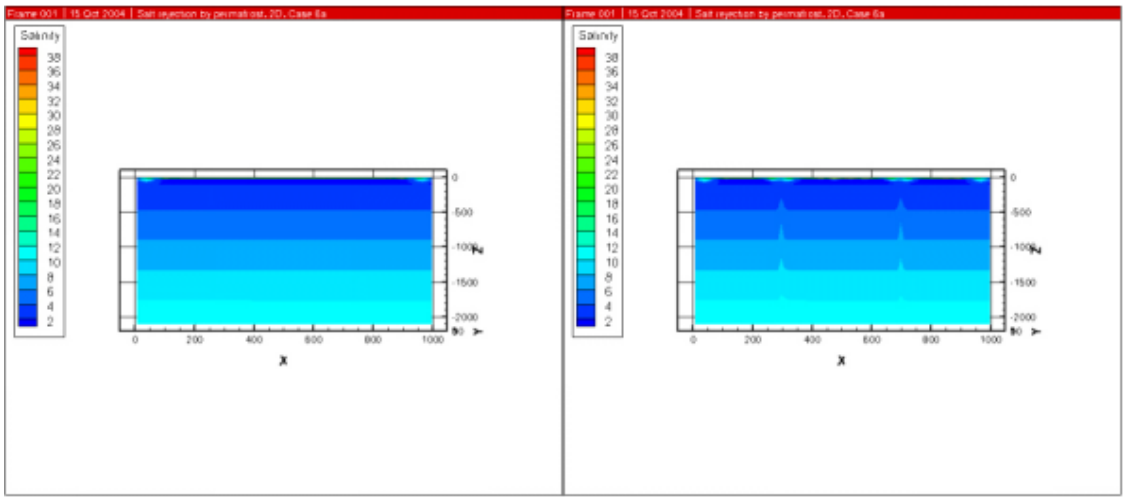

Figure 3-2b. *Salinity distribution after six months for (left) homogeneous model and (right) homogeneous model traversed by two vertical fracture zones. In the figures z=0 corresponds to the bottom of the permafrost, and not to ground surface.*

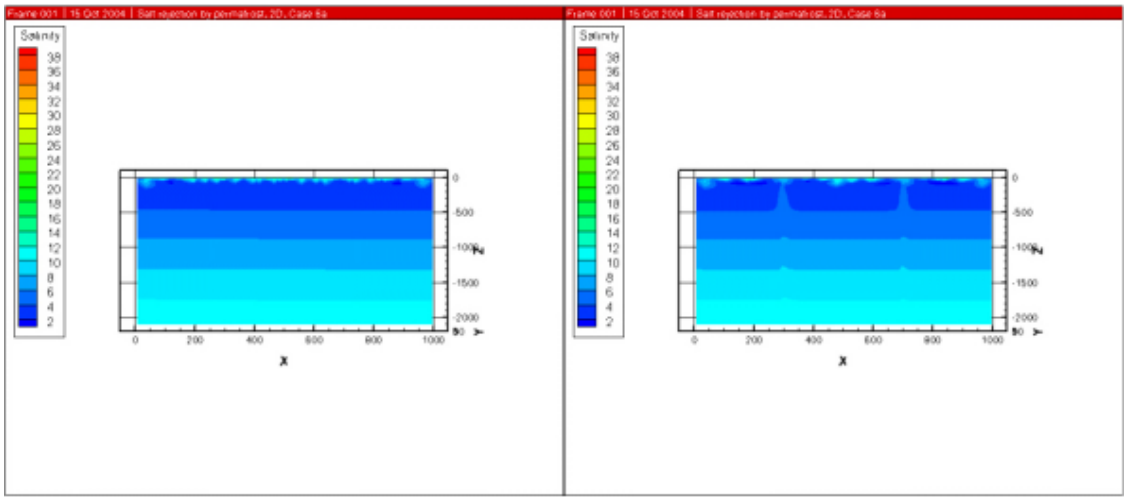

Figure 3-2c. *Salinity distribution after one year for (left) homogeneous model and (right) homogeneous model traversed by two vertical fracture zones. In the figures z=0 corresponds to the bottom of the permafrost, and not to ground surface.*

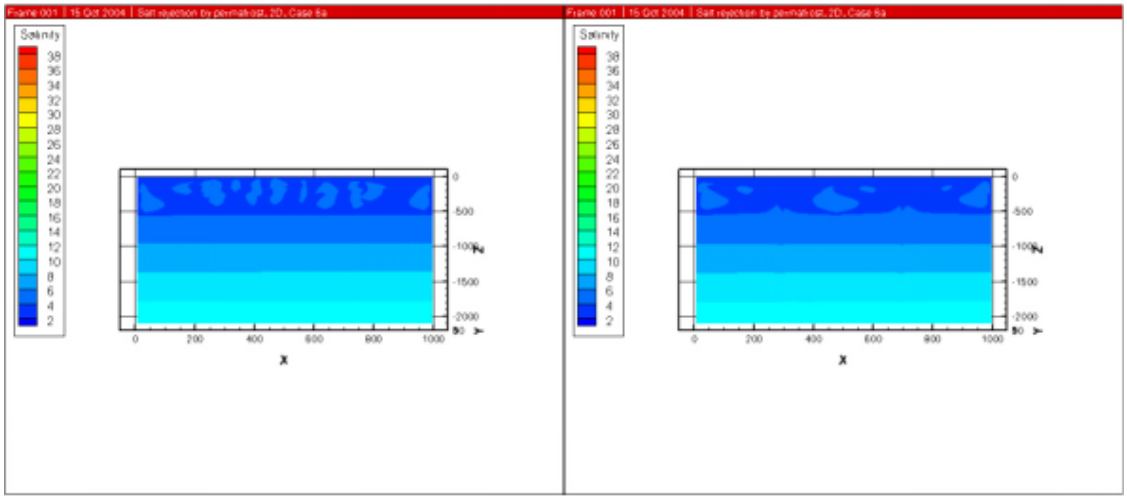

Figure 3-2d. *Salinity distribution after five years for (left) homogeneous model and (right) homogeneous model traversed by two vertical fracture zones. In the figures z=0 corresponds to the bottom of the permafrost, and not to ground surface.*

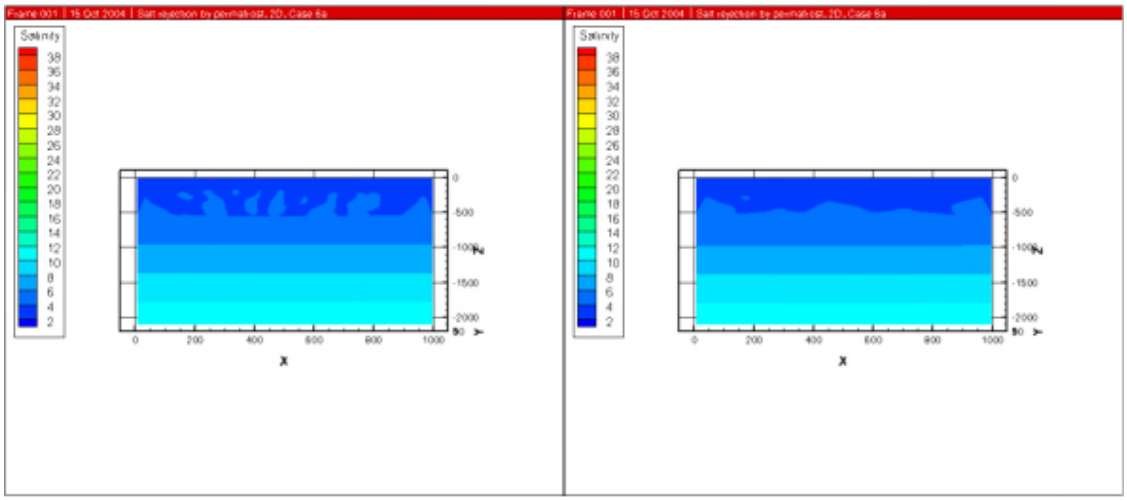

Figure 3-2e. *Salinity distribution after ten years for (left) homogeneous properties and (right) homogeneous traversed by two vertical fracture zones. In the figures z=0 corresponds to the bottom of the permafrost, and not to ground surface.*

In comparing the results presented in Figure 3-2a–e it is conclusive that the occurrence of fracture zones initiates the mixing process so that mixing starts earlier Than in the case of a "perfect" homogeneous model Also the fracture zones will contain a larger part of the mixed water. The rock mass between the deterministic deformation zones is hence less affected by the downward moving saline waters if fracture zones exist.

The second series of simulations investigate the influence due to a regional flow across the model domain. The simulated cases are of an idealised fractured bedrock containing two fracture zones. The hydraulic conductivity of the fracture zones is in this case approximately three orders of magnitude larger than in the previous case. This idealised fractured bedrock contains two fracture sets – one horizontal and one vertical – and fractures with lengths within the interval 10–200 m are generated using a power-law relation established from field data at the Äspö HRL /Darcel 2003/. The basis for the generated hydraulic conductivity and porosity values are an empirical relationship from field data at Äspö HRL between fracture length (size) and fracture transmissivity along with a relationship between fracture transmissivity and transport aperture /Vidstrand 2004/. The resulting hydraulic conductivity of the bedrock is somewhat larger than the homogeneous case presented above. The calculated porosity is of the same order. For the cases of regional flow (right illustrations in Figures 3-3 to 3-4e) an in-flux on the left-hand side, decreasing with depth, is specified so that the resulting regional gradient at the surface is approximately 0.01 [m/m]. The used gradient is decreasing with depth due to the salinity stratification.

The simulations with a regional groundwater flow gradient suggest that a regional flow due to flushing decreases the portion of high saline water reaching deeper parts of the model domain. In the performed simulations the water that comes into the model is fixed at the same salinity as the initial salinity profile. Therefore an influence of rejected salt upstream the model domain is neglected. It could be expected that this neglection causes an under-estimation of available high saline waters. The effect of such under-estimation has not been investigated. One could however speculate that some fracture zone geometries would support a longer time feed of high saline waters yielding a longer mixing period.

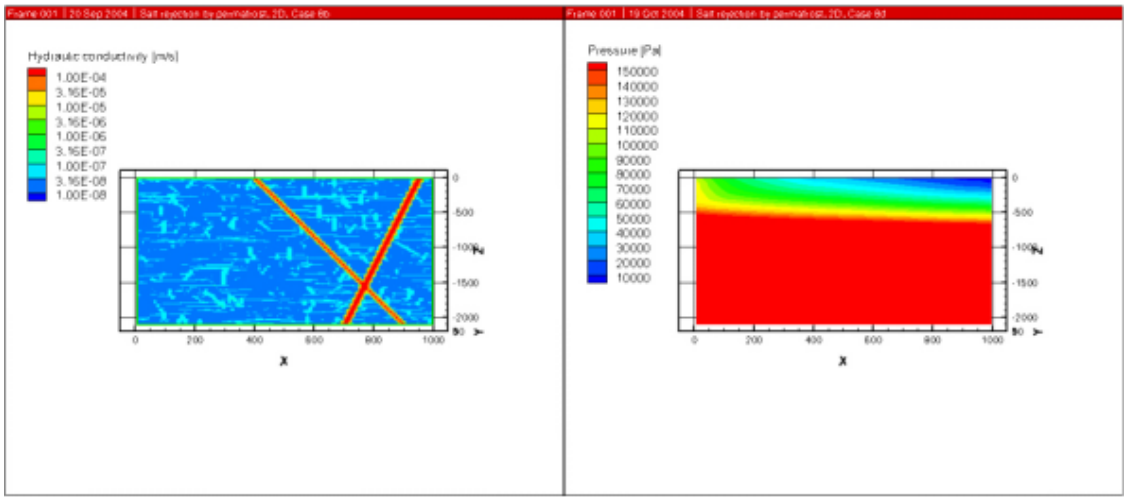

Figure 3-3. *Hydraulic conductivity of the fracture network (left) and the pressure distribution for the case of regional flow (right). In the figures z=0 corresponds to the bottom of the permafrost, and not to ground surface.*

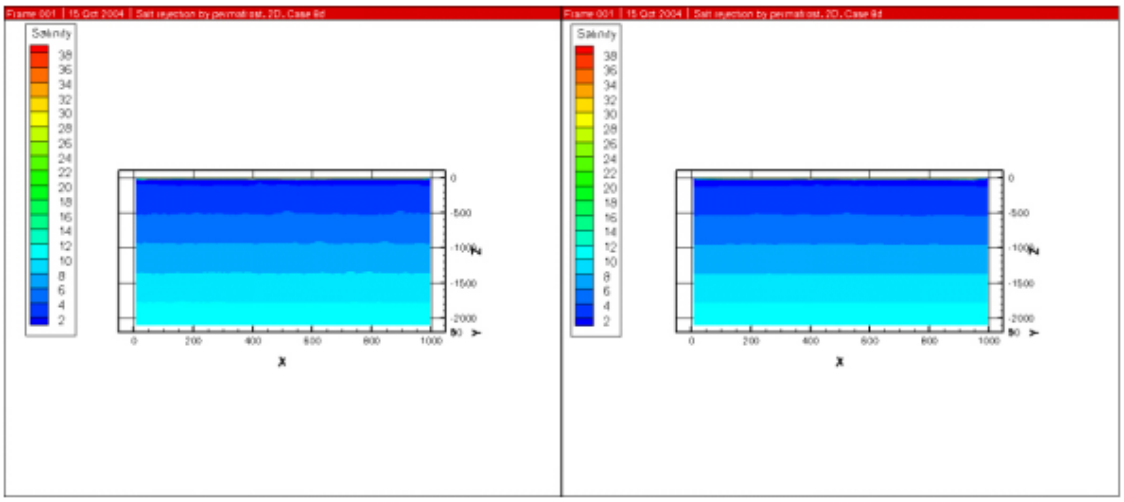

Figure 3-4a. *Salinity distribution after one month for a fractured network traversed by fracture zones with no regional flow boundary (left) and with a regional flow boundary (right). The properties and flow characteristics are presented in Figure 3-3. In the figures z=0 corresponds to the bottom of the permafrost, and not to ground surface.*

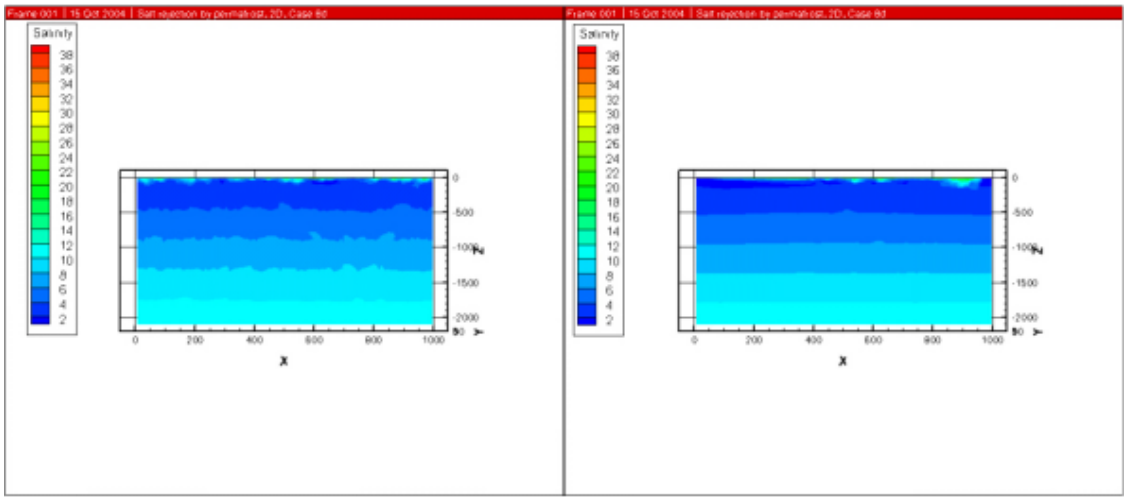

Figure 3-4b. *Salinity distribution after six months for a fractured network traversed by fracture zones with no regional flow boundary (left) and with a regional flow boundary (right). The properties and flow characteristics are presented in Figure 3-3. In the figures z=0 corresponds to the bottom of the permafrost, and not to ground surface.*

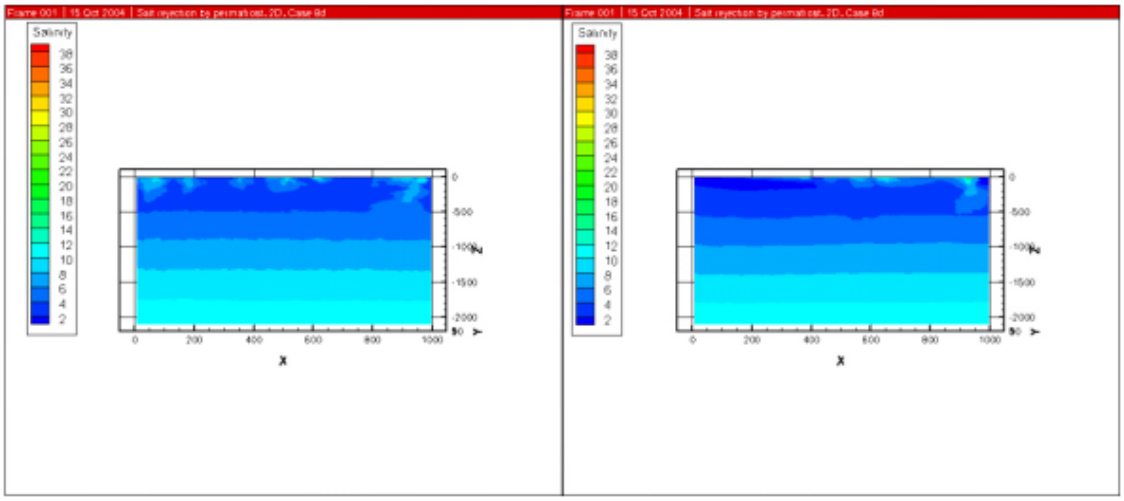

Figure 3-4c. *Salinity distribution after one year for a fractured network traversed by fracture zones with no regional flow boundary (left) and with a regional flow boundary (right). The properties and flow characteristics are presented in Figure 3-3. In the figures z=0 corresponds to the bottom of the permafrost, and not to ground surface.*

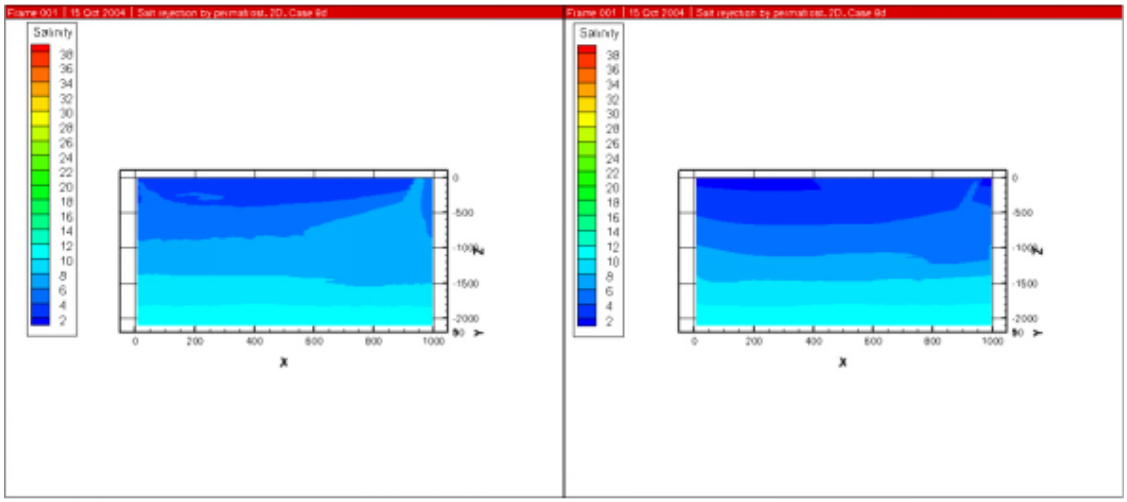

Figure 3-4d. *Salinity distribution after five years for a fractured network traversed by fracture zones with no regional flow boundary (left) and with a regional flow boundary (right). The properties and flow characteristics are presented in Figure 3-3. In the figures z=0 corresponds to the bottom of the permafrost, and not to ground surface.*

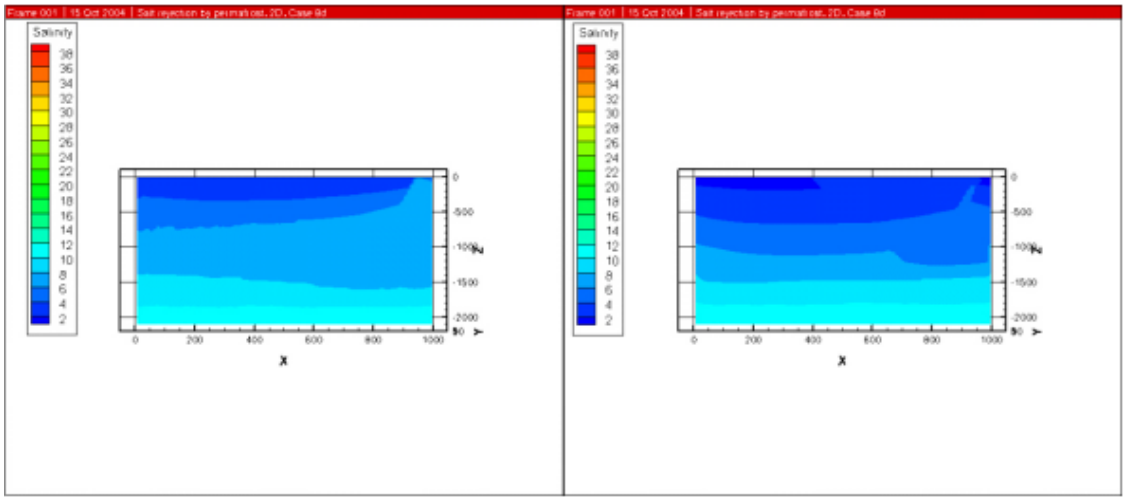

Figure 3-4e. *Salinity distribution after ten years for a fractured network traversed by fracture zones with no regional flow boundary (left) and with a regional flow boundary (right). The properties and flow characteristics are presented in Figure 3-3. In the figures z=0 corresponds to the bottom of the permafrost, and not to ground surface.*

4 Model setup and specifications

Since this study adopted the geometrical models and boundary conditions from the POM v1.1 model /Follin et al. 2004/, it does not contain the general assessments of geometrical alternatives, uncertainties of boundary conditions and parameter values along with model calibrations.

Brief descriptions of geometrical model and boundary conditions of the modelled area are presented below.

4.1 Modelling methodology

The modelling methodology used in this study follows SKB's system approach for hydrogeological modelling /Rhén et al. 2003/. This approach divides the geosphere into three types of Hydraulic Domains, representing the Quaternary deposits (HSD), the fracture zones (HCD), and the rock mass between the fracture zones (HRD), see Figure 4-1.

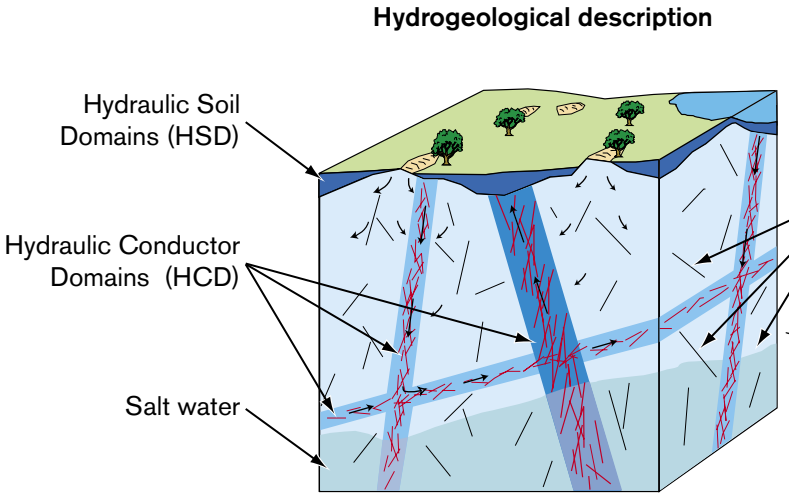

Figure 4-1. *The Quaternary deposits and the crystalline bedrock are divided into separate hydraulic domains named Hydraulic Soil Domains (HSD), Hydraulic Rock Mass Domain (HRD), and Hydraulic Conductor Domains (HCD). Within each domain the hydraulic properties are represented by mean values or by spatially distributed statistical distributions. After /Rhén et al. 2003/.*

4.2 Site description

Figure 4-2 shows the extent and dimension of the model domain used. The elevation data is presented on-top of the deterministically defined deformation zones. These deformations zones are shown in Figure 4-3 and Table 4-1 and Table 4-2 present the statistical information of the stochastic deformation zones. Table 4-3 present the hydraulic properties of deformation zones and the background fracture network (smaller than simulated). Model domain origin is found at 1539000 (x=0), 6360000 (y=0) in RT90 with no rotation.

The diffusive exchange of salt between the pore volumes containing mobile water and the pore volumes of immobile water – matrix diffusion – is modelled as a multi-rate diffusion process /Haggerty and Gorelick 1995, Svensson et al. 2004/. One of the key parameters in this multi-rate conceptualisation is the capacity ratio between immobile and mobile volumes. It is assumed that the immobile water volume is 10–100 times the mobile water volume; in our main simulation the ratio is set to ten (10). The effect of different ratios is investigated as a sensitivity study.

Table 4-1. Spatial model, stochastic fracture (deformation zone) intensity, and fracture size distribution.

Parameter	Type/value
Spatial model (initial)	Poisson
Intensity (P_{32c}) [m^2/m^3]	0.0371
Fracture length (size) distribution	Power-law
Smallest length (size) (L_0) [m]	100
Power-law slope (CCDF $k_{L,3D}$)	2.6

Table 4-2. Pole orientation and relative proportions of stochastic fracture (deformation zones) sets.

Fracture set	Mean pole trend	Mean pole plunge	Dispersion	Distribution	% of fractures
1	262.0	3.8	8.52	Fisher	24.9
2	195.9	13.7	9.26	Fisher	32.1
3	135.9	7.9	9.36	Fisher	25.9
4	35.4	71.4	7.02	Fisher	17.1

Table 4-3. Hydraulic properties of the bedrock.

Feature	Transmissivity/hydraulic conductivity/porosity	Comments
Deterministic deformation zones	$1.3 \cdot 10^{-05}$ [m^2/s]	
Stochastic deformation zones	$T = a \cdot L^b$ [m^2/s]	a = $2.47 \cdot 10^{-5}$, b = 1.791. L represents stochastic deformation zone length (size).
Background rock mass (lowest hydraulic conductivity)	$1.0 \cdot 10^{-12}$ [m/s]	
Superficial rock mass	$1.0 \cdot 10^{-09}$ [m/s]	Not used within modelled domain
Average kinematic porosity	$2–4 \cdot 10^{-04}$ [–]	Calculated
Average matrix proosity	$2–4 \cdot 10^{-03}$ [–]	Calculated

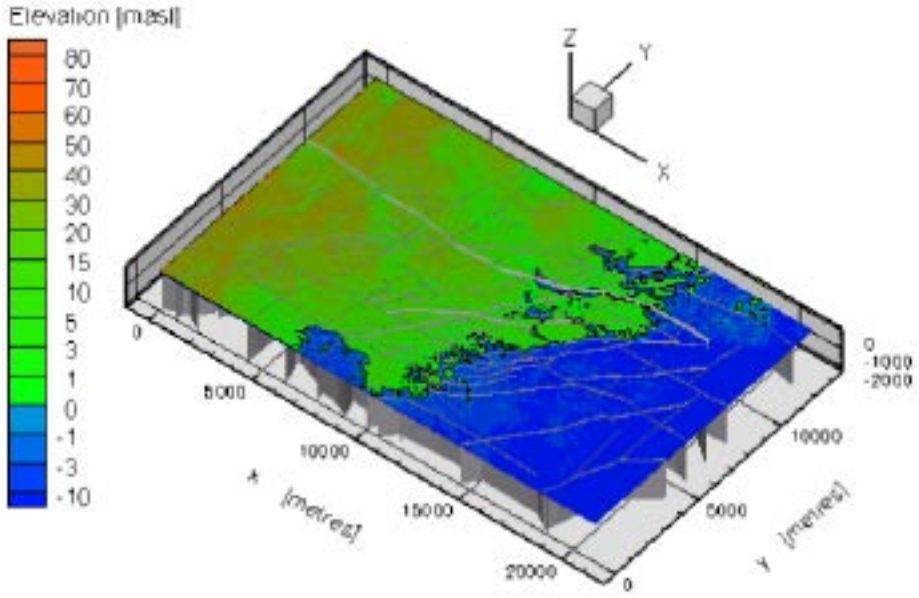

Figure 4-2. *Dimensions of the regional model domain to scale (POM v1.1). The bottom boundary is located 2,100 m depth (below sea level (sea level equals zero elevation). The outcropping of the deterministically modelled deformation zones in shaded grey. The dimensions of the entire model are 21 km (x-direction), 13 km (y-direction), and approximately 2.1 km (z-direction).*

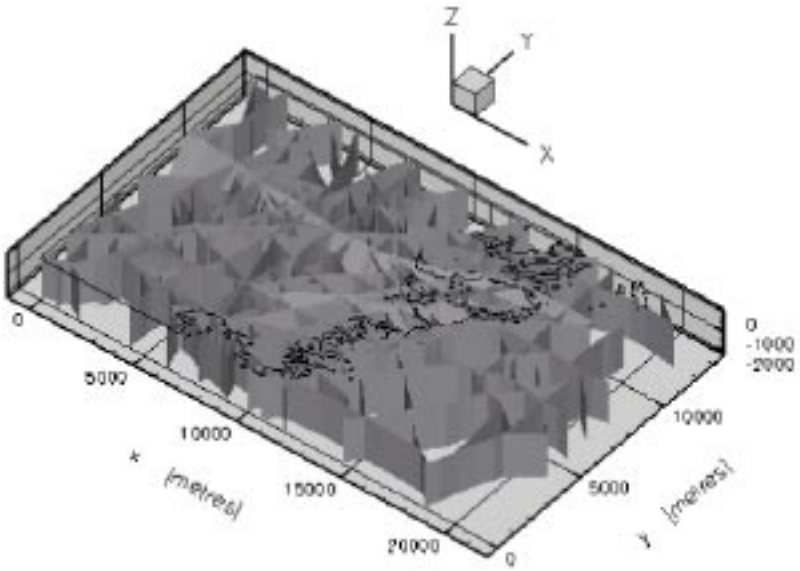

Figure 4-3. *Overview of the deterministically modelled deformation zones (based on the V0 deformation zone model).*

4.3 Surface processes and initial conditions

The initial salinity condition, before the onset of permafrost, constitute a linear increasing salinity from zero salinity at sea level to 10% by weight at 2,100 m depth.

The temperature field is based on results from permafrost growth simulations for the Laxemar region /SKB 2006/ and kept constant over the simulation (both the Laxemar and the Simpevarp sites are found within the regional model domain). The original curved data have been simplified to fit two straight lines with the a gradient of approximately 25.7 degrees per kilometre in the top kilometre and below that a gradient of approximately 24.6 degrees per kilometre.

Ice crystals can not accommodate dissolved chemical species. As a consequence the remaining liquid phase will experience an aggradation of chemical components, of which salt is one component. This salt aggradation of salt in the unfrozen groundwater is commonly referred to as salt rejection. Of the permafrost processes possible, only the process of salt rejection was considered in the study.

In the numerical simulations this process was assumed to produce a "spike" of high saline waters directly beneath the permafrost. The spike was assumed to occur instantaneously down to different depths: 50, 150 or 300 m. The selected permafrost depth stays fixed over the entire simulation. The high saline pulse is only released within the mobile water volume. As a consequence the matrix diffusion has a significant effect on the salinity within the release layer.

The value (in percentage by weight) of the high salinity pulse was calculated based on the amount of available salt (in relation to the initial salinity profile described above) within the depth interval subjected to freezing by permafrost. The available salt was calculated within the code and the rejected salt was placed beneath the permafrost, see Tables 4-4 to 4-5.

The rejected salt is assumed to be re-distributed in a 10 m thick layer just beneath the permafrost.

The maximum salinity in groundwater based on the solubility of NaCl in water is between 30 and 40% depending on among other factors the temperature; water at 20°C could reach a salinity of 36%.

Table 4-4. Available salt and average porosity within the permafrost layer.

Permafrost depth [m]	Mass of rejected salt [kg]	Average porosity [–]
50	$1.81 \cdot 10^{8}$	$4.612 \cdot 10^{-4}$
150	$2.45 \cdot 10^{9}$	$4.085 \cdot 10^{-4}$
300	$2.26 \cdot 10^{10}$	$3.931 \cdot 10^{-4}$

Table 4-5. Initial salinity value of the high saline pulse released in the layer just beneath the permafrost layer.

Permafrost depth [m]	Salinity [%] by weight
50	0.4
150	3.0
300	22.4

4.4 Boundary conditions

The adopted boundary conditions from the POM v1.1 model constitute a no-flow condition on all lateral sides and at the bottom. Within the POM v1.1 model local and regional fluxes were created by the fixed pressure at the topographical surface. Topographical differences, i.e. gradients, are small compared to permafrost thicknesses. The depth of the Baltic Sea within the model domains is also small. Therefore it is assumed that at the bottom of the permafrost, topographical differences at the surface can be neglected. The permafrost is assumed impervious and the surface boundary is also a no-flow boundary in the permafrost simulations herein presented.

Since the topographical influence is neglected, and no in-flux occurs at the lateral side boundaries no regional flow is simulated. As a consequence, the flow within the model is as a consequence driven by density differences only.

4.5 Time step dependence

Simulations in order to test the dependence of model results of the size of the time step have been performed. The result are found to be converging even though a small difference is still apparent with time steps on the daily scale. A time step of approximately 7 days (0.02 year) is chosen for the simulations. In all simulations a coupled pressure-salinity equation is solved in order to obtain somewhat better results.

As illustrated in Figure 4-4a–b the results at 460 m depth are not so affected by the time step length on a scale shorter than approximately one month. However, in the release layer (Figure 4-4c and Figure 4-5) small differences are apparent still on the time scale of days.

The chosen main setting yielded computer run times of approximately 70 hours for a 300 years simulation. The sensitivity runs takes approximately 2.5 hours for a 10 years simulation. The majority of the sensitivity runs are performed as 10 years simulations. The background fracture network takes approximately one hour to generate.

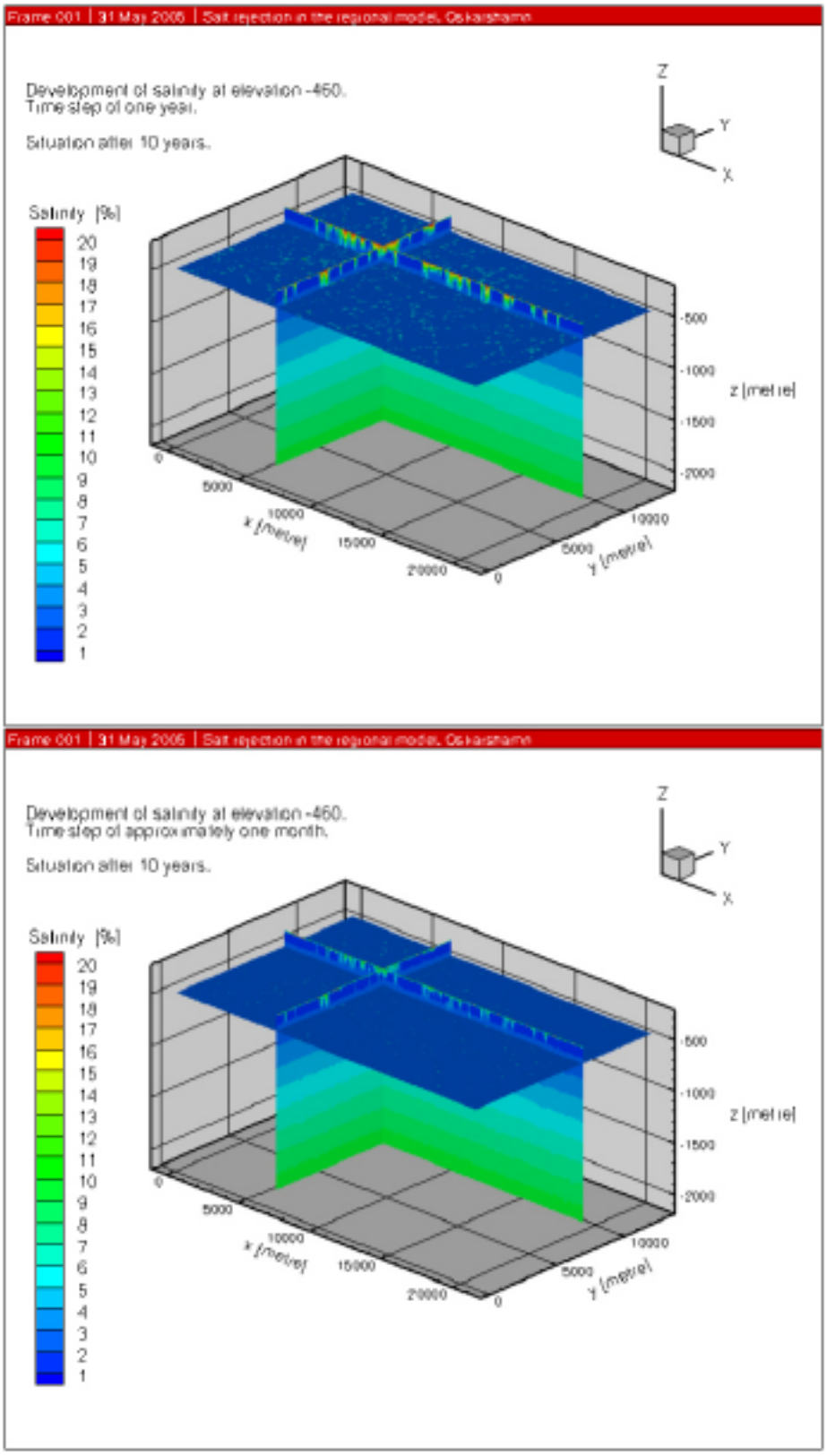

Figure 4-4a. *Illustration of time step dependency.*

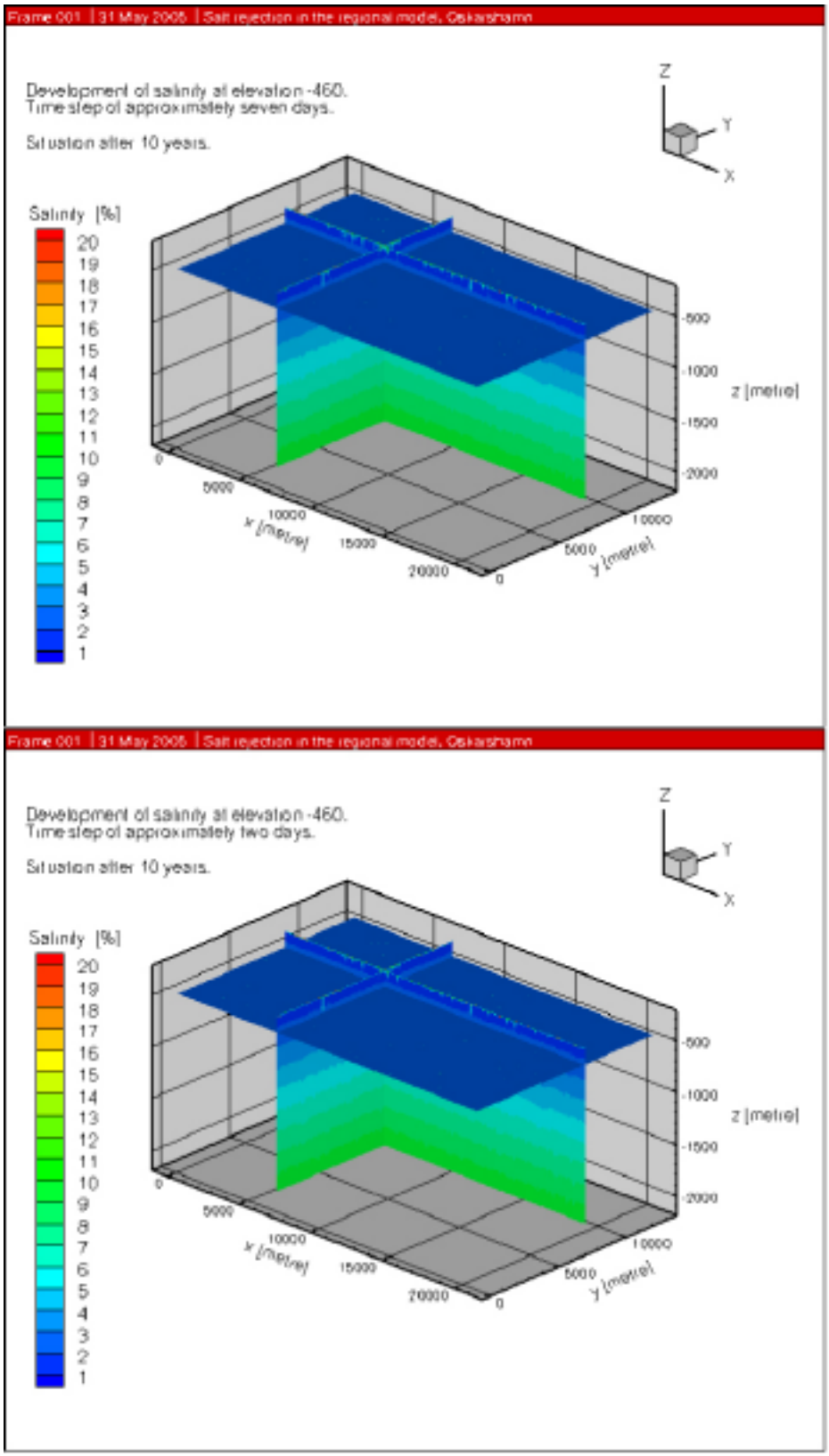

Figure 4-4b. *Illustration of time step dependency.*

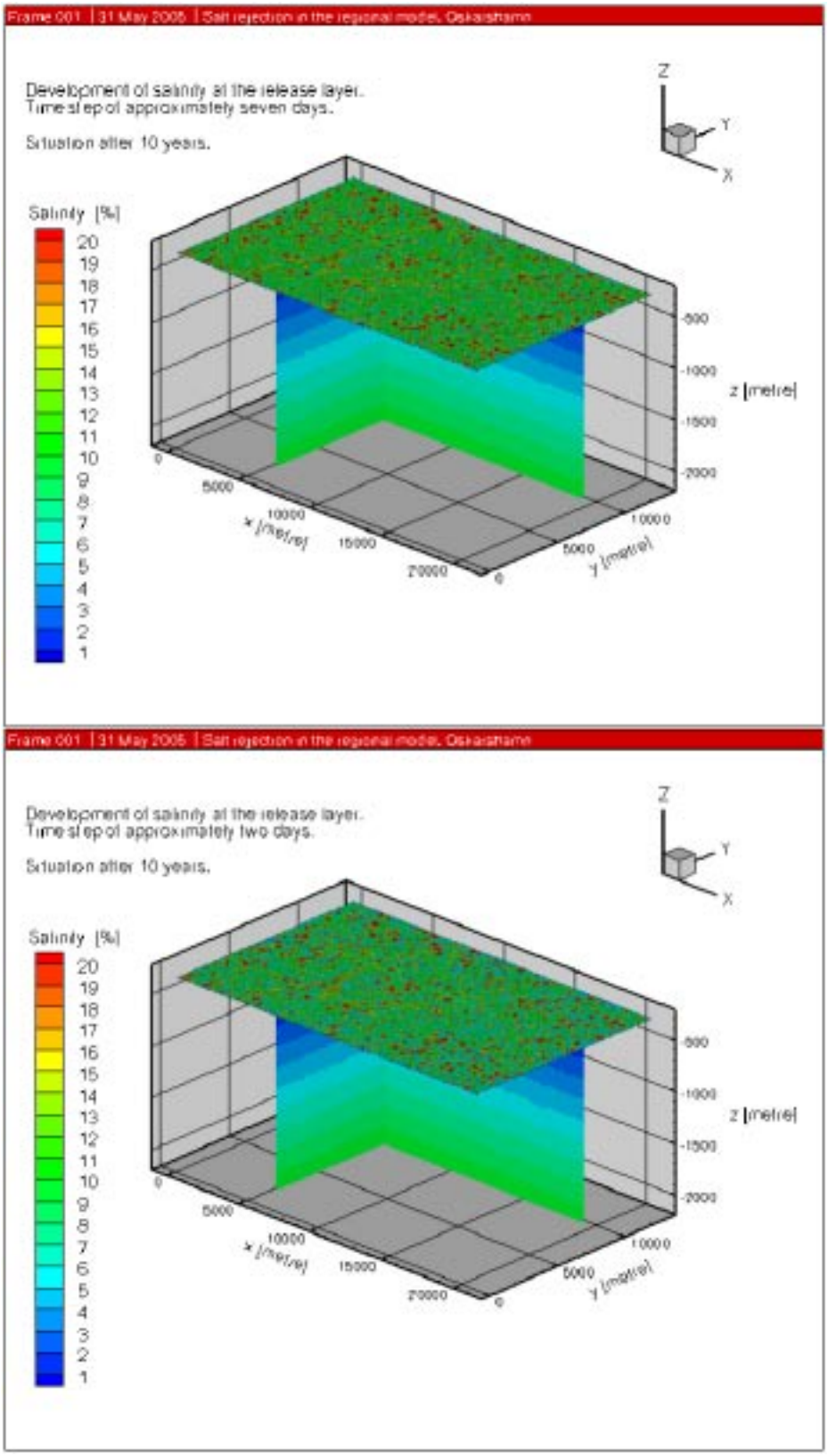

Figure 4-4c. *Illustration of time step dependency.*

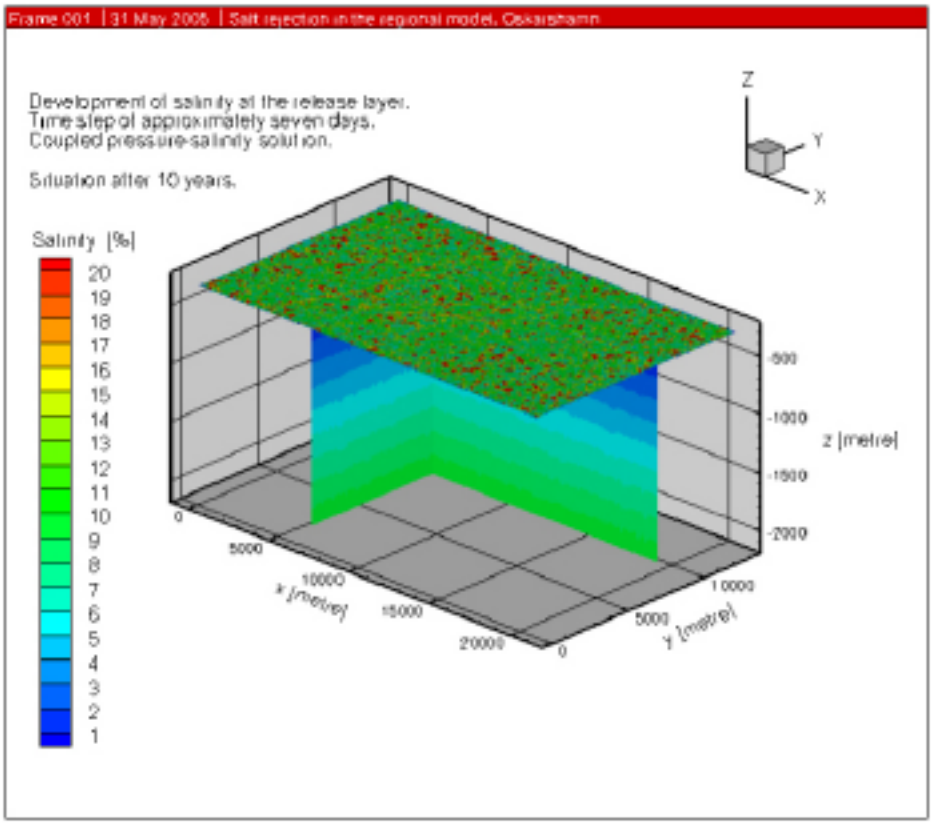

Figure 4-5. *Illustration of the effect of a coupled pressure-salinity solution on time step dependency.*

4.6 Deliverables

The deliverables of the study are the development of the salinity field after an initial pulse of high saline water is released beneath a permafrost layer.

5 Result of transient simulations

All presented results are based on the simulation of permafrost reaching a depth of 300 m. The initial pulse of more saline waters for the other cases, where the permafrost reached less depth, is much smaller. Additional, the 300 m depth corresponds, within some tenths of metres, to the maximum modelled permafrost depth for Laxemar during a 120,000 year long simulated glacial cycle with chosen environmental conditions exceptionally favourable for permafrost growth /SKB 2006/.

Figure 5-1 presents an illustration of the salinity distribution after three-hundred years.

Figure 5-2a–d present the development of the groundwater salinity at 310 m depth, that is 10 m below the level at which the high salinity pulse was released. Figure 5-2a shows the initial salinity conditions one layer beneath the one containing the salt rejected by permafrost. The following Figure 5-2b–d show how the saline water flows down (during 15 years) within the more permeable deformation zones, but also how the low-permeable surrounding rock mass between the deformation zones experiences an almost negligible salinity increase even though it is only 10 m between numerical cell centres in the vertical direction.

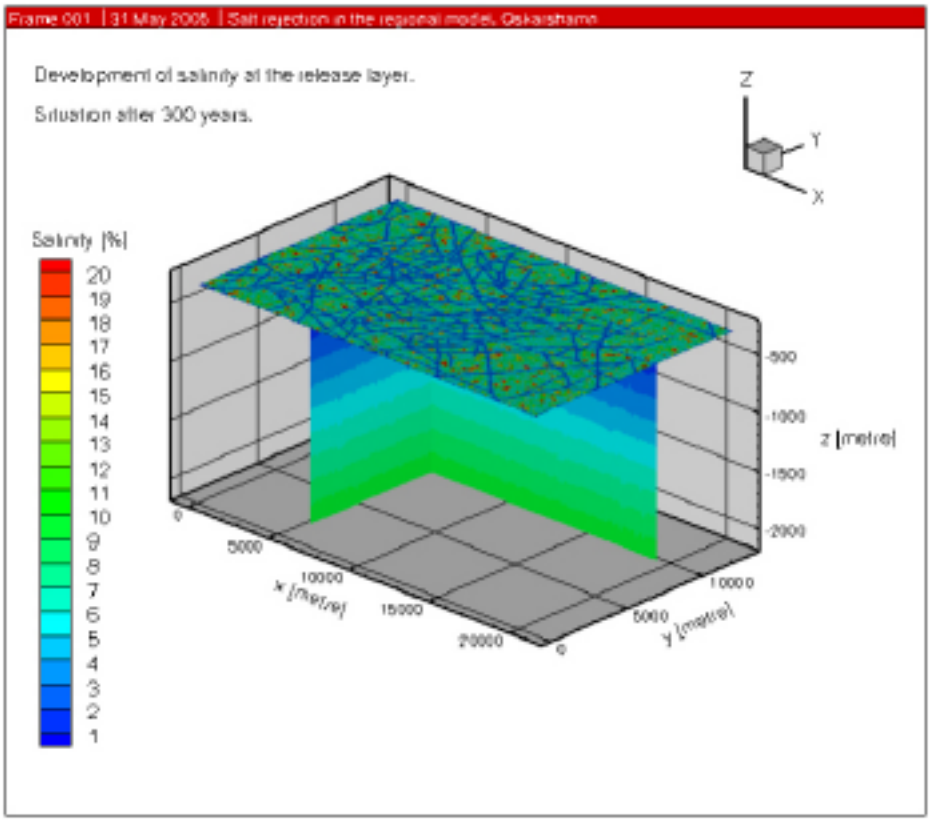

Figure 5-1. *Illustration of the salinity distribution in the model domain after 300 years.*

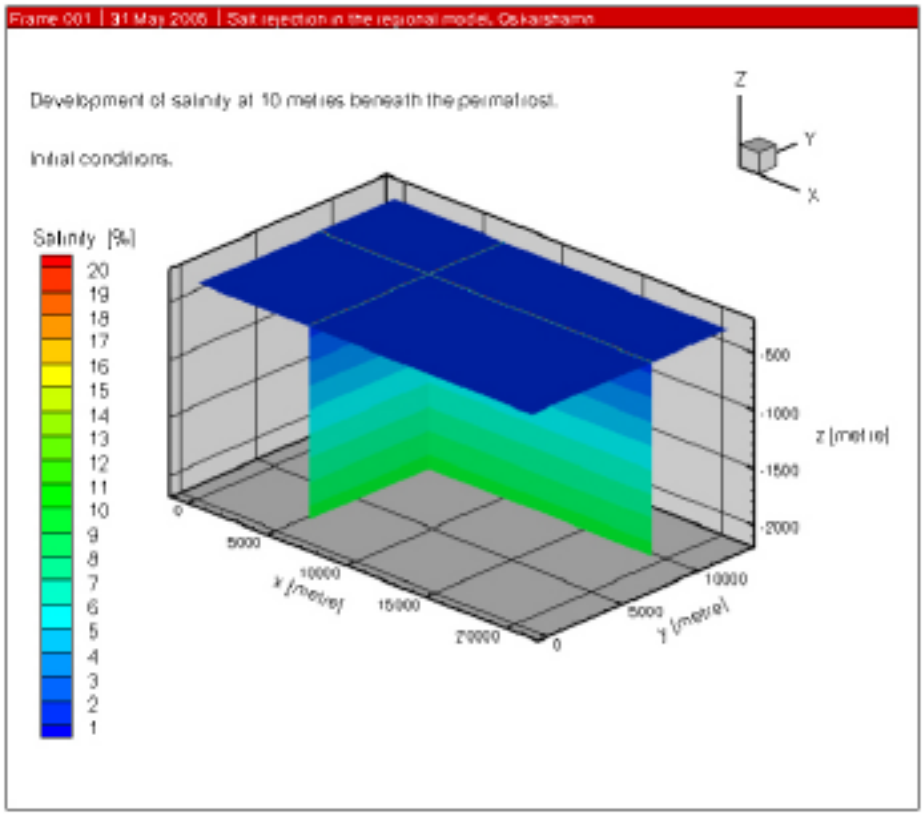

Figure 5-2a. *Initial salinity [%] distribution at 310 m depth. This illustration presents the initial salinity conditions one layer beneath the release of the saline water. The following Figure 5-2b–d will show how the saline water flow down (during 15 years) within the more permeable deformation zones, but also how the low-permeable surrounding bedrock between the deformation zones experience small if any salinity increase even though it is only 10 m between numerical cell centres in the vertical direction.*

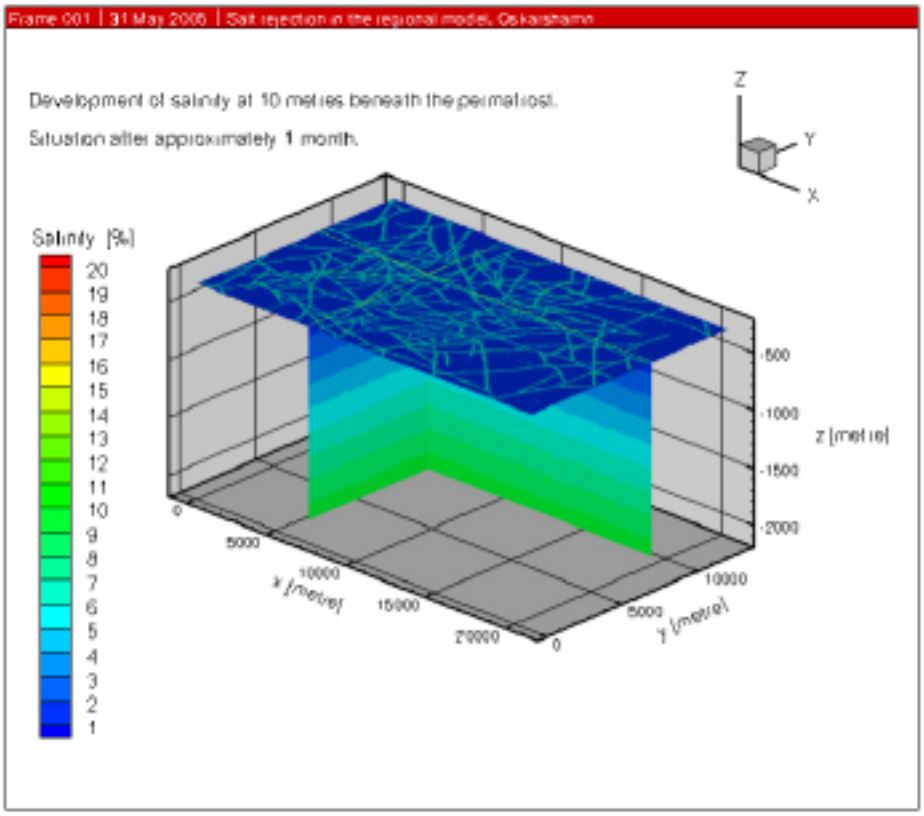

Figure 5-2b. *Salinity [%] distribution at 310 m depth after approximately one month.*

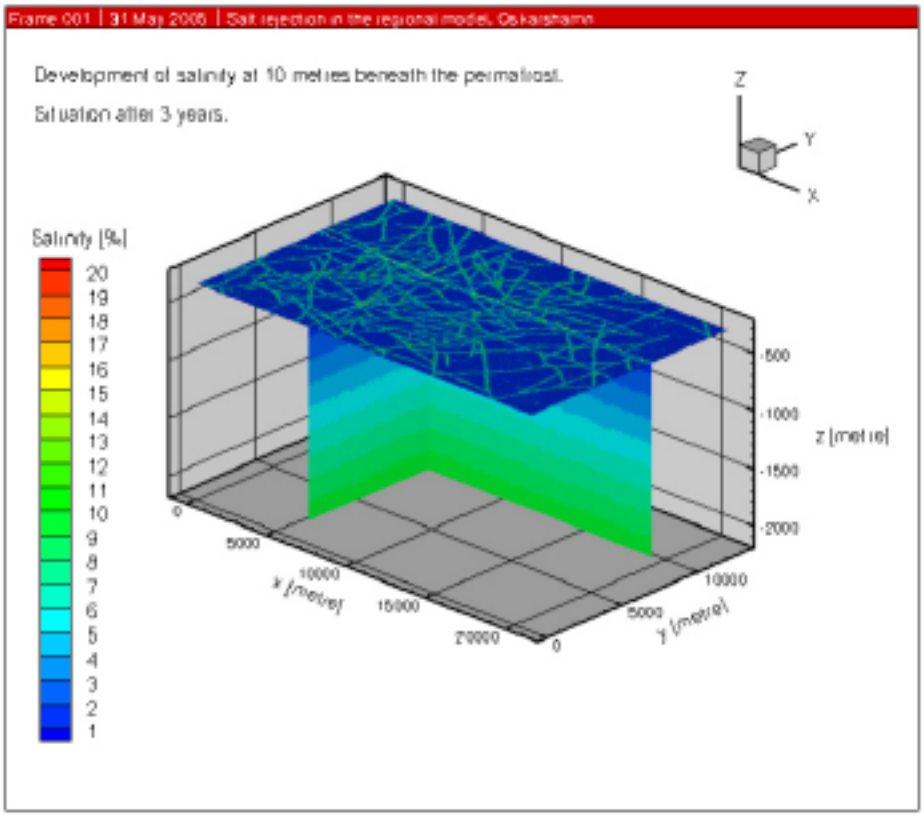

Figure 5-2c. *Salinity [%] distribution at 310 m depth after three years.*

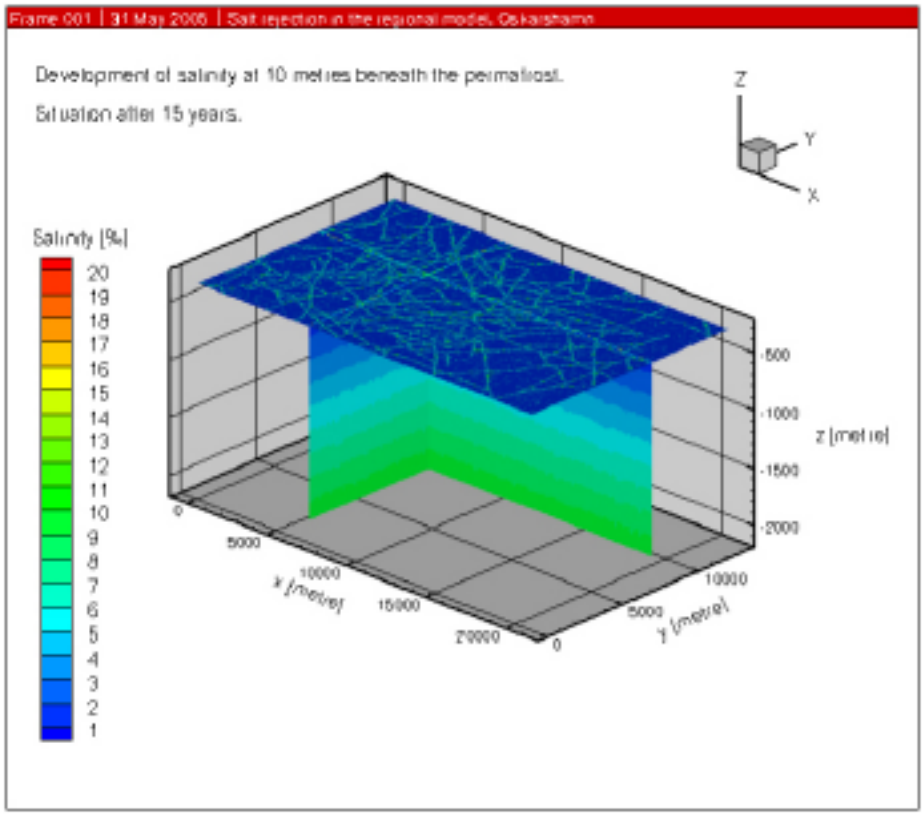

Figure 5-2d. *Salinity [%] distribution at 310 m depth after fifteen years.*

The results indicate that the maximum salinity values some ten metres below the permafrost will be around 10% for an initial value of approximately 22%. Further, the results indicate that the salinity values within the deformation zones have started to decrease after 15 years.

Figure 5-3a–d present the development (during 300 years) of the groundwater salinity at 460 m depth, i.e. 160 m below the level at which the high salinity pulse was released.

The results indicate that the maximum salinity values at approximately 150 m below the permafrost will reach values just below 10%. However the spatial pattern of these high salinity values are not an exact reflection of the deformation zones. Although contained within the deformation zones, the high salinity values are mostly located at deformation zone crossings.

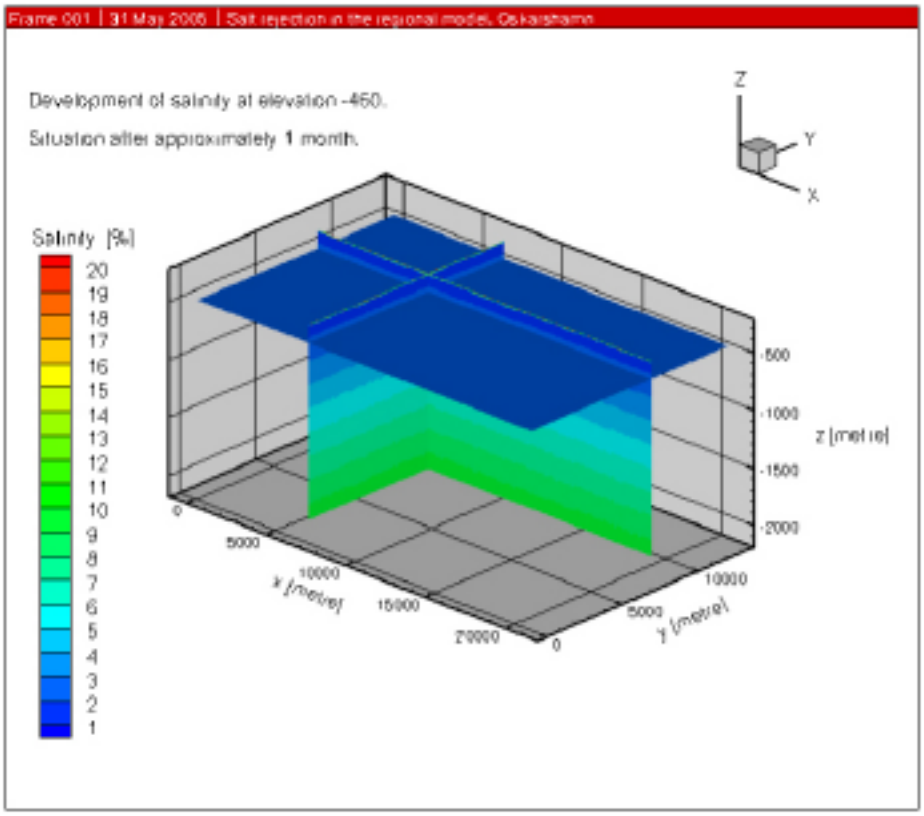

Figure 5-3a. *Salinity [%] distribution at 460 m depth after approximately one month. This illustration presents the initial salinity conditions approximately 150 beneath the release of the saline water. The following Figure 5-3b–d will show how the saline water flows down (during 300 years) within the more permeable deformation zones, but also how the low-permeable surrounding bedrock in between the deformation zones experience small if any salinity increase.*

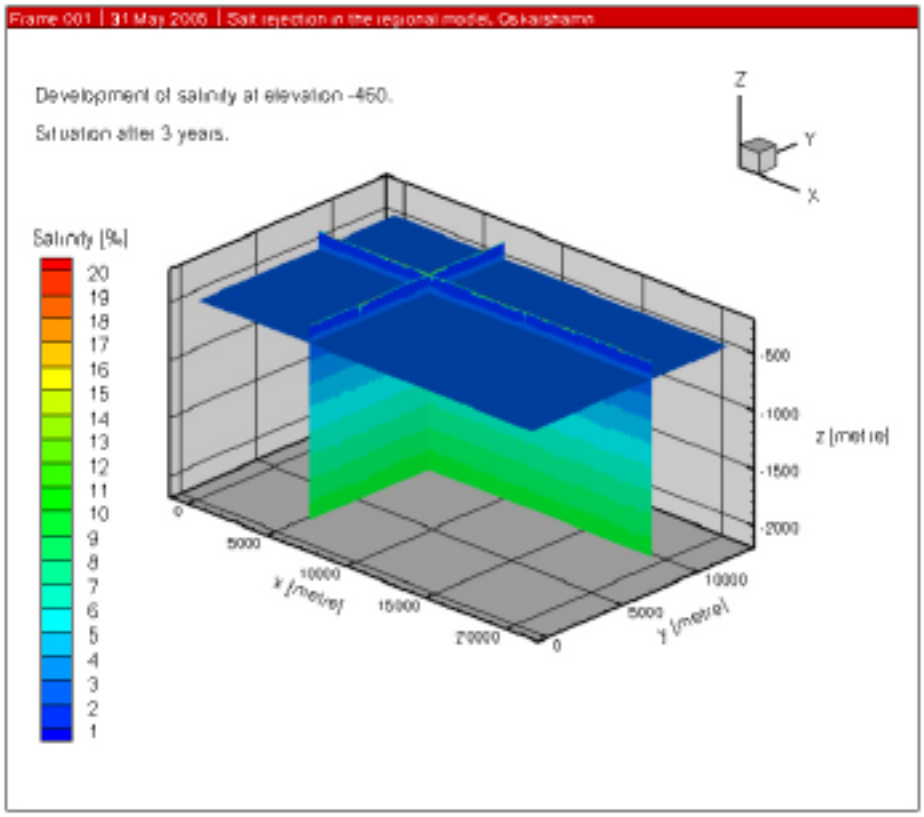

Figure 5-3b. *Salinity [%] distribution at 460 m depth after three years.*

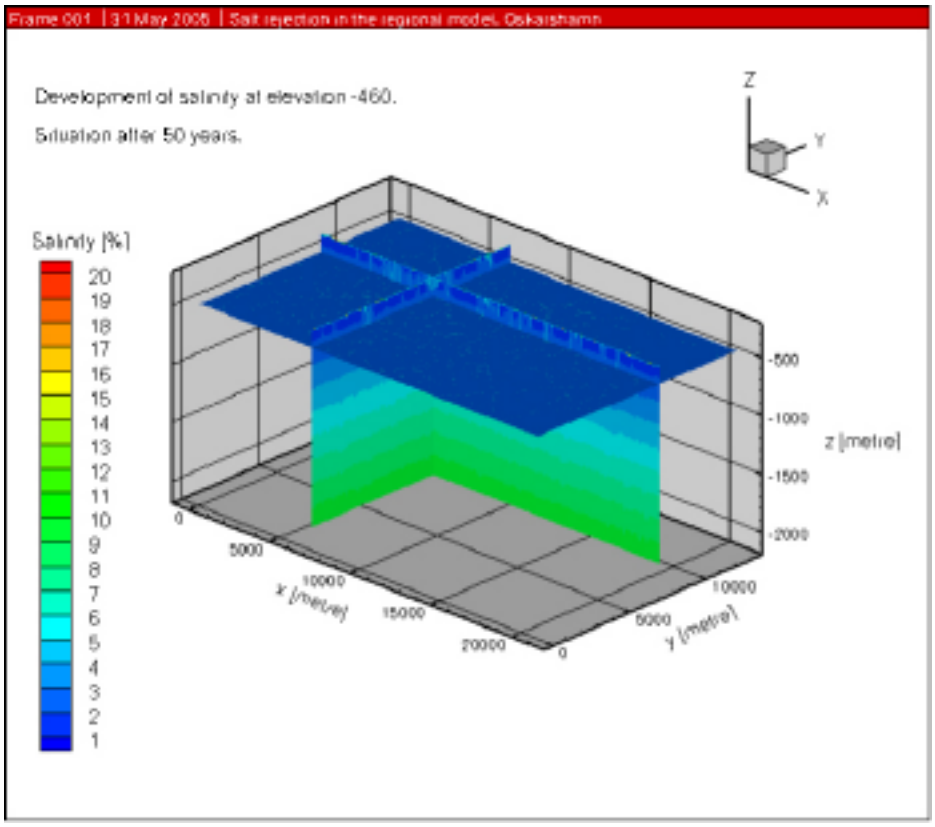

Figure 5-3c. *Salinity [%] distribution at 460 m depth after fifty years.*

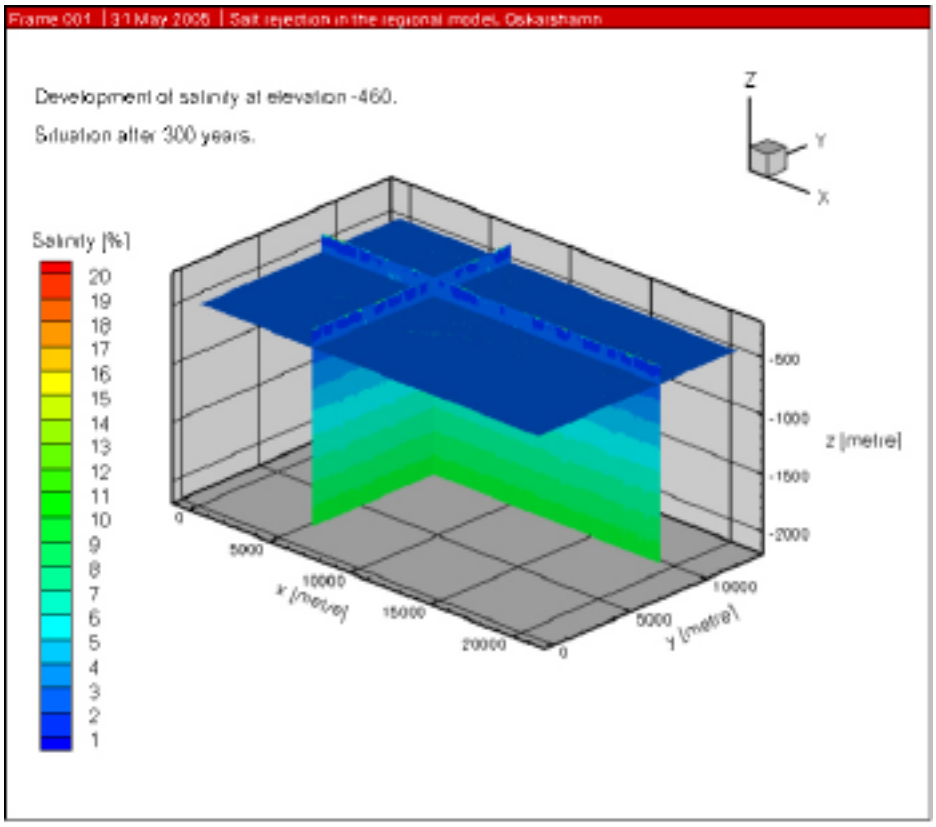

Figure 5-3d. *Salinity [%] distribution at 460 m depth after three-hundred years.*

Figure 5-4a–f present illustrations of salinity values, for all data points at 460 m depth in relation to permeability at the point, for different times. The results shown in these figures show that the maximum salinity values found at elevation −460 m reach values just below 10 % in the first tens of years (10–30 years). Thereafter the maximum salinity values decrease.

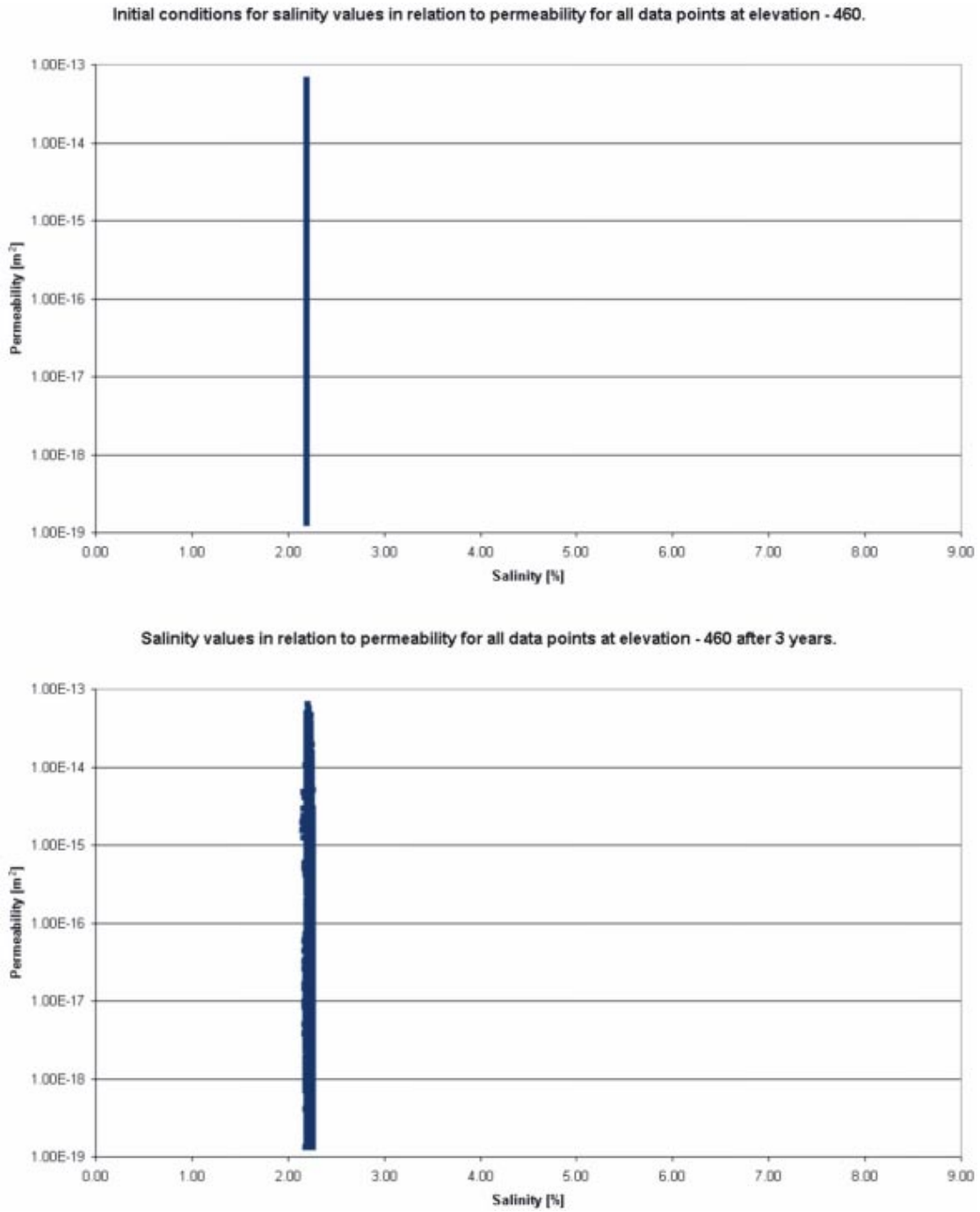

Figure 5-4a. *Salinity values in relation to permeability for all data points at elevation –460 m. The Figure 5-4a–f illustrate a transient of the salinity on elevation –460 for a series of different times. The data are presented in a cross-plot of permeability value in the numerical cell and salinity value in the same numerical cell. As can be seen in the Figure sequence the more permeable parts of the network contain the majority of saline downward flow.*

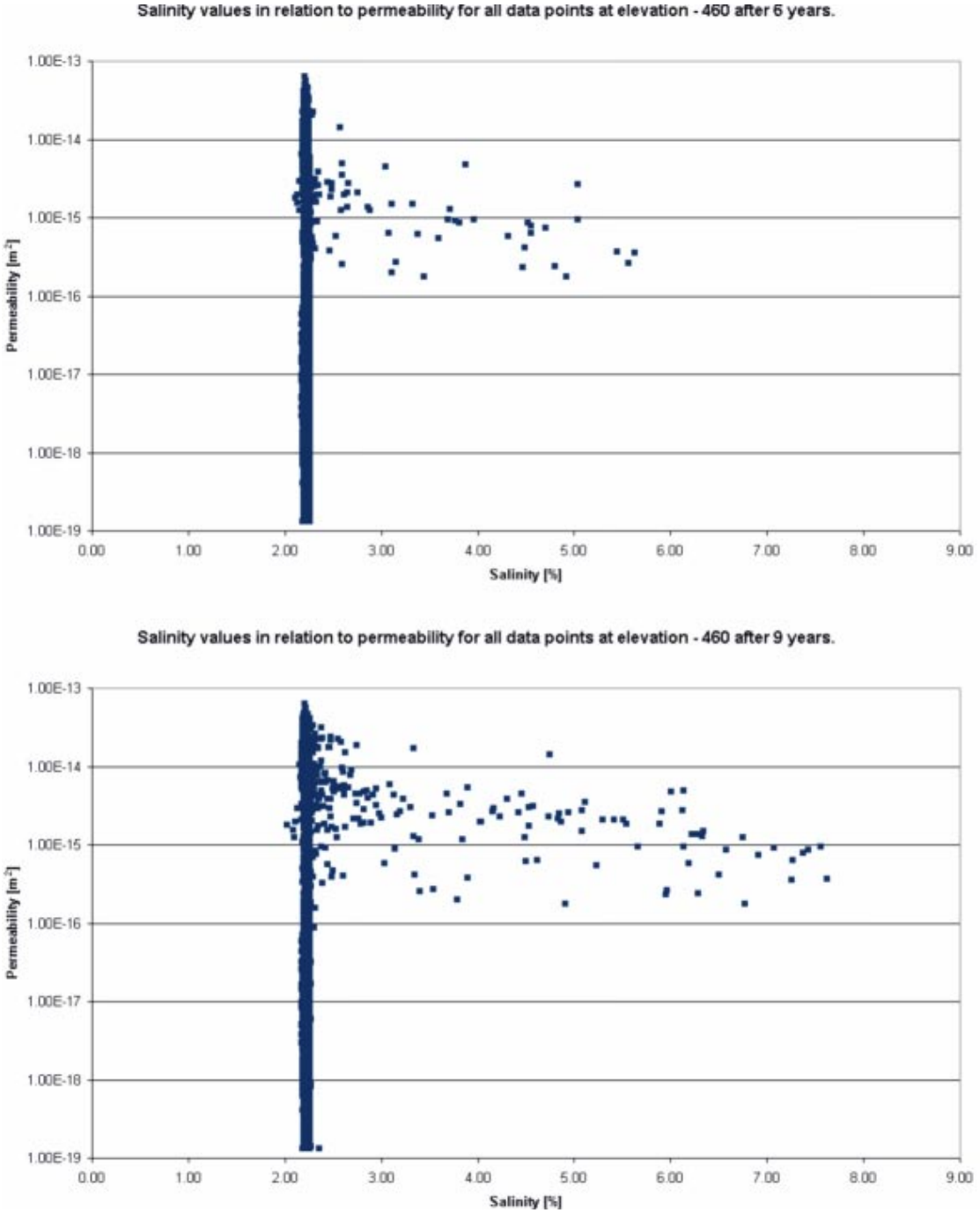

Figure 5-4b. *Salinity values in relation to permeability for all data points at elevation –460 m.*

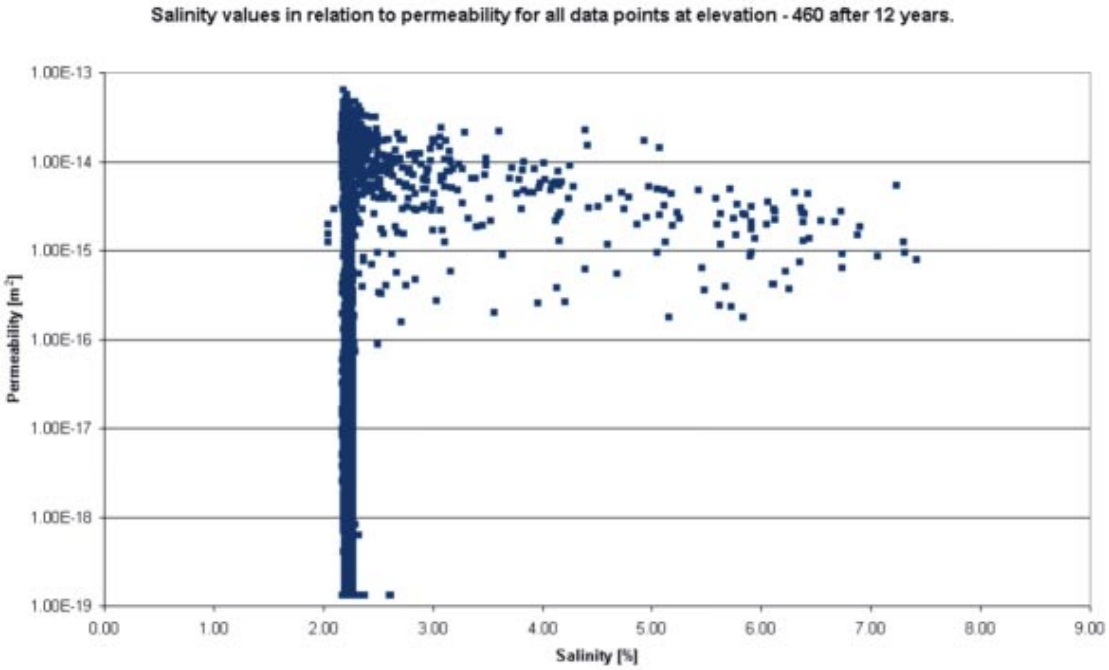

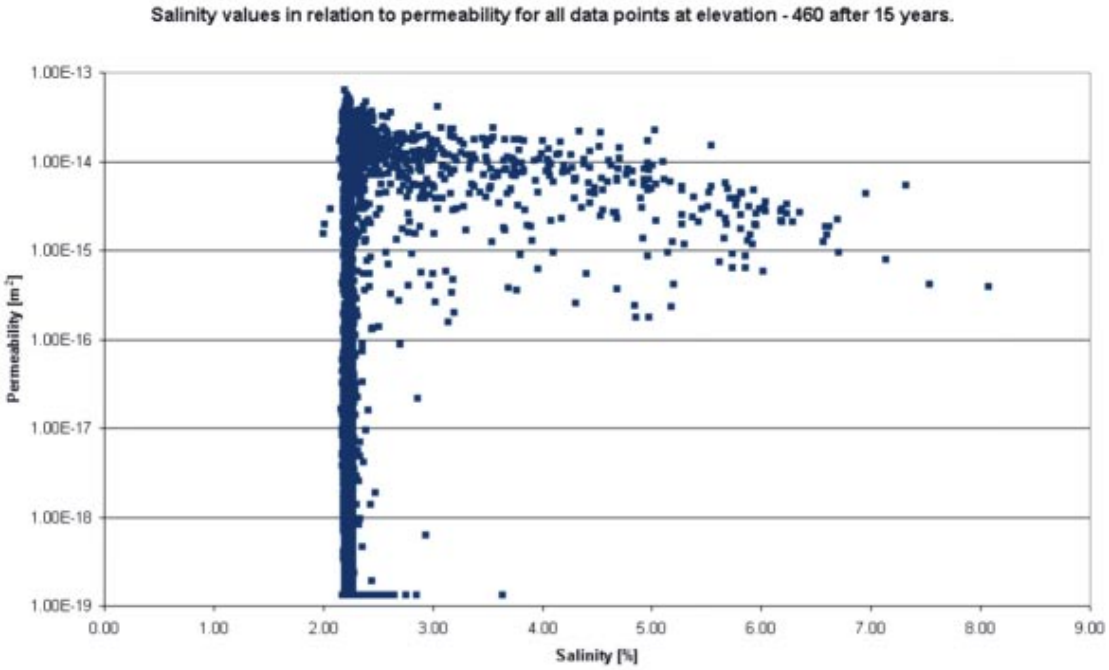

Figure 5-4c. *Salinity values in relation to permeability for all data points at elevation –460 m.*

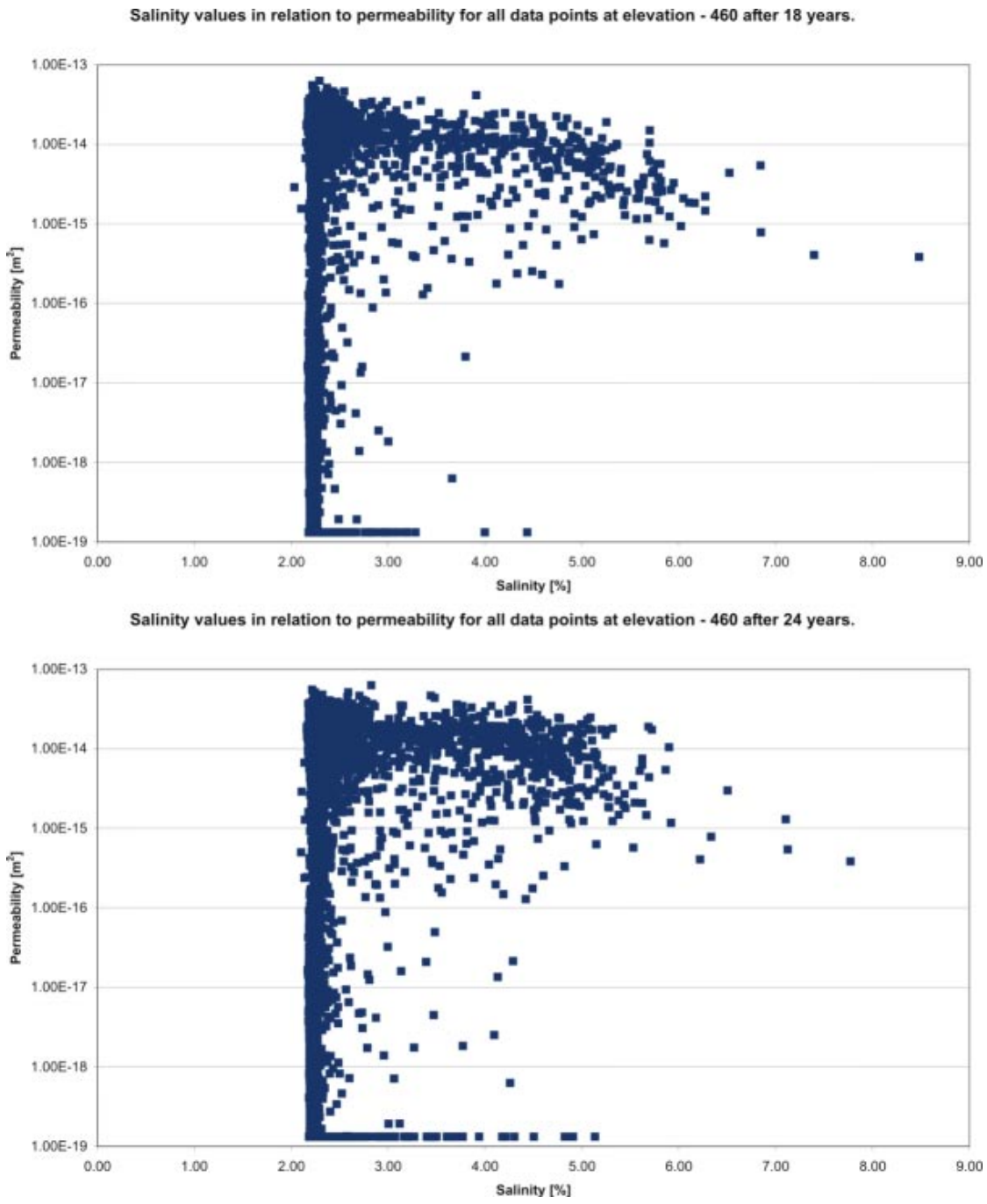

Figure 5-4d. *Salinity values in relation to permeability for all data points at elevation –460 m.*

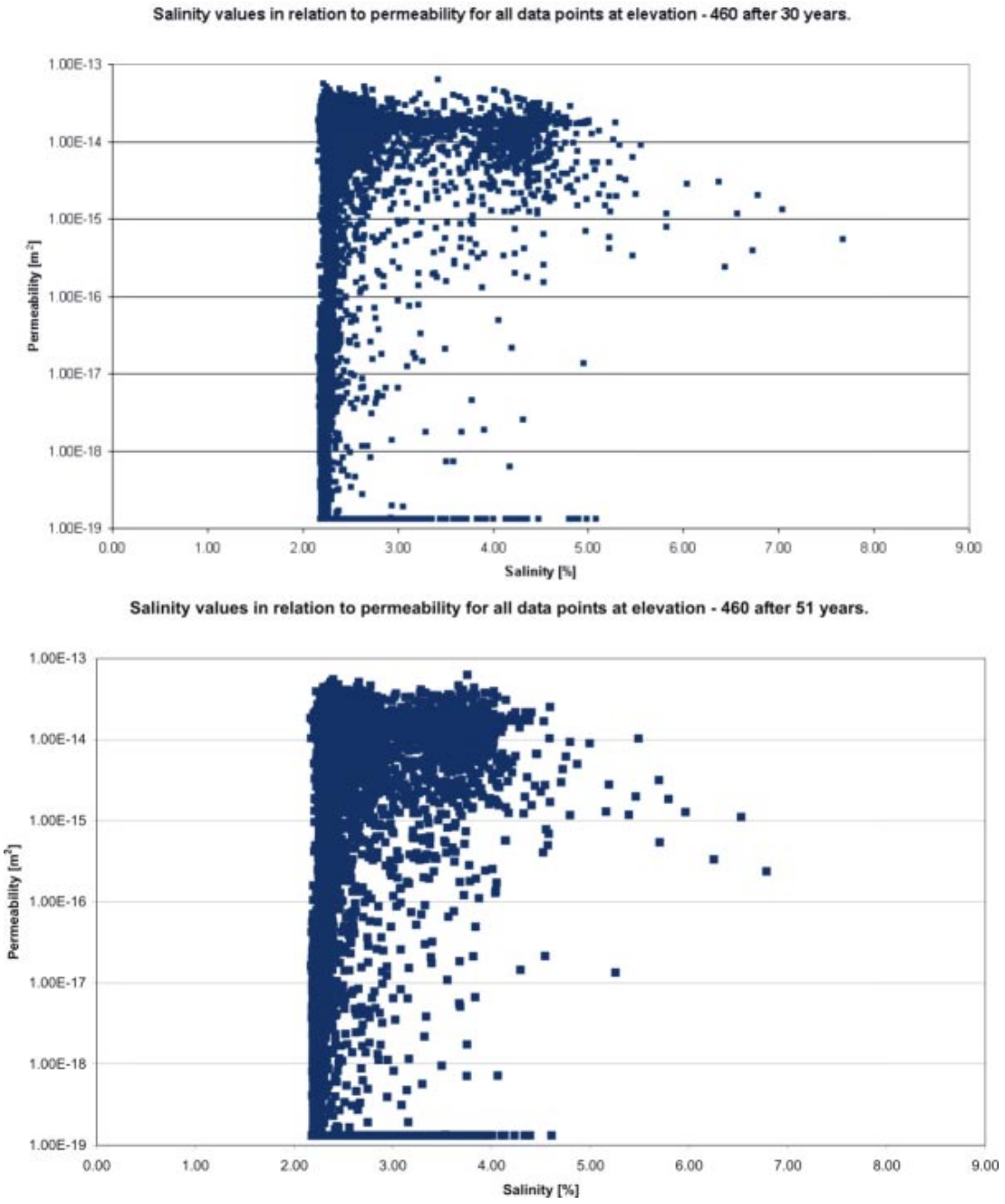

Figure 5-4e. *Salinity values in relation to permeability for all data points at elevation –460 m.*

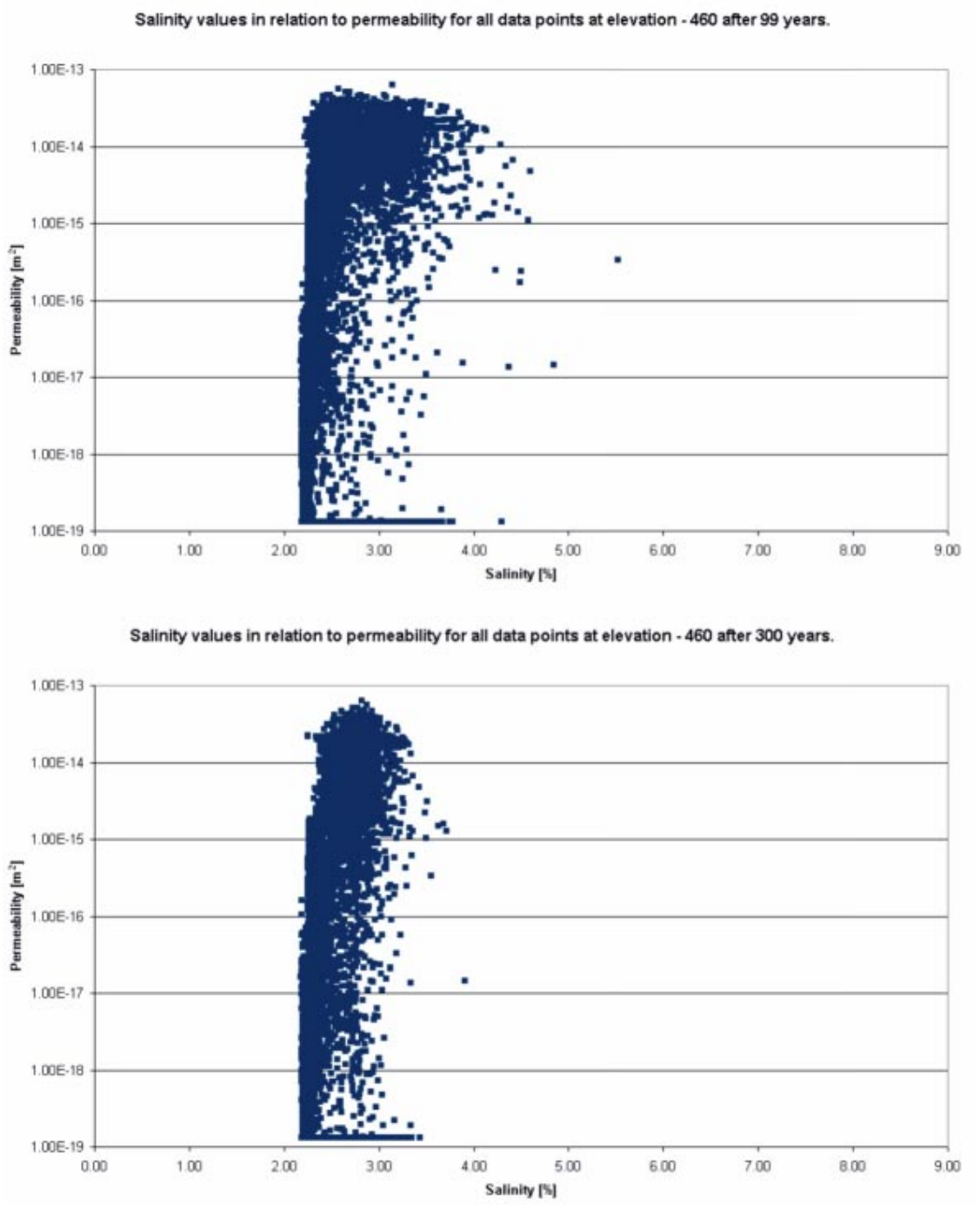

Figure 5-4f. *Salinity values in relation to permeability for all data points at elevation –460 m.*

Figure 5-5a presents the results of the salinity development at nine different locations at which maximum salinity is reached at different times. Figure 5-5b–c present spatial distribution of some interesting locations in regards to salinity values.

In Figure 5-5a the development of salinity with time is illustrated for nine different locations that experience the highest salinity at elevation –460 for different times. The anomaly seen for the tightest bedrock that also contains some relative early salinity increase is further illustrated in Figure 5-5b. The locations for the first salinity increase are presented in Figure 5-5c.

The locations of tight bedrock with relatively early salinity increase are seen in Figure 5-5b. It is satisfying that all of these locations are found in direct connections with the more permeable cells that contains the deterministic deformation zones that also are the most permeable parts of the model domain. The greyish network in Figure 5-5b–c is created with permeability values larger than $1 \cdot 10^{-15}$ [m^2/s]. In Figure 5-5c it is suggested that the locations of the earliest salinity increase are found within the deterministic deformation zones and that a majority of these locations also have a correlation with deterministic deformation zone crossings.

Figure 5-6a–b present the main component of the direction of the flow along with Darcy velocity values for two cross-sections at the level of 460 m depth. In Figure 5-6a–b it is seen that only the deterministic deformation zones contain the majority of the flow, presented as Darcy velocities. These figures also show that the zones include regions of both upward and downward flow; that is the convection cells developed are principally contained within the more permeable parts.

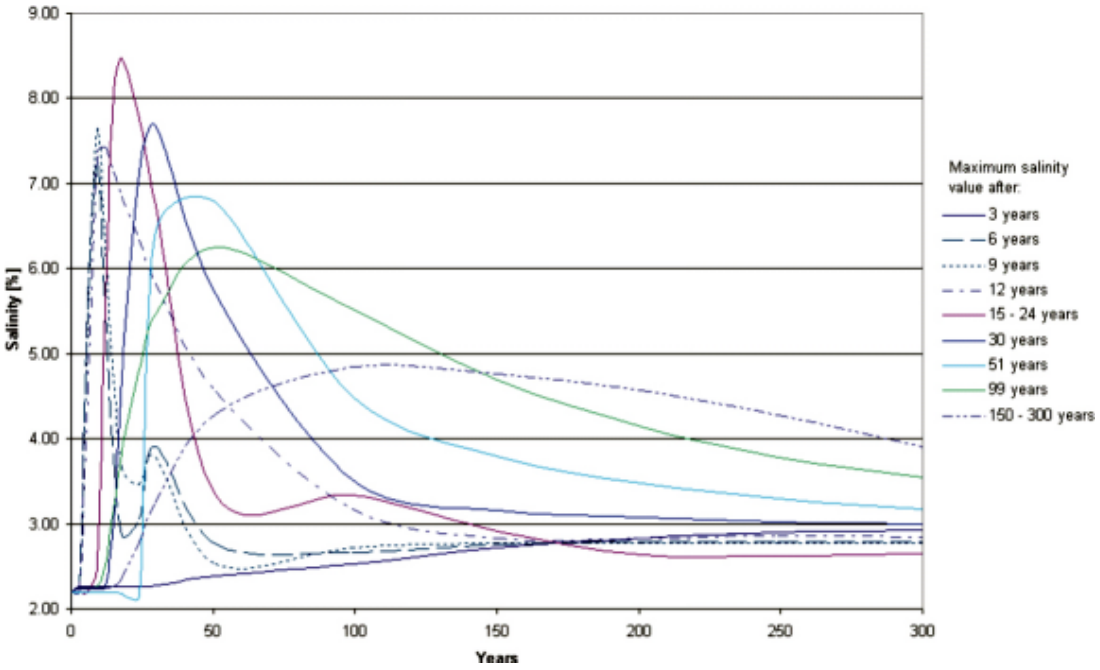

Figure 5-5a. *Salinity development at nine different locations at 460 m depth for which the related maximum value of the depth was after 3, 6, 9, 12, 15–24, 30, 51, 99, and 150–300 years, respectively. The location was found after searching for maximum values at the chosen depth for different time steps.*

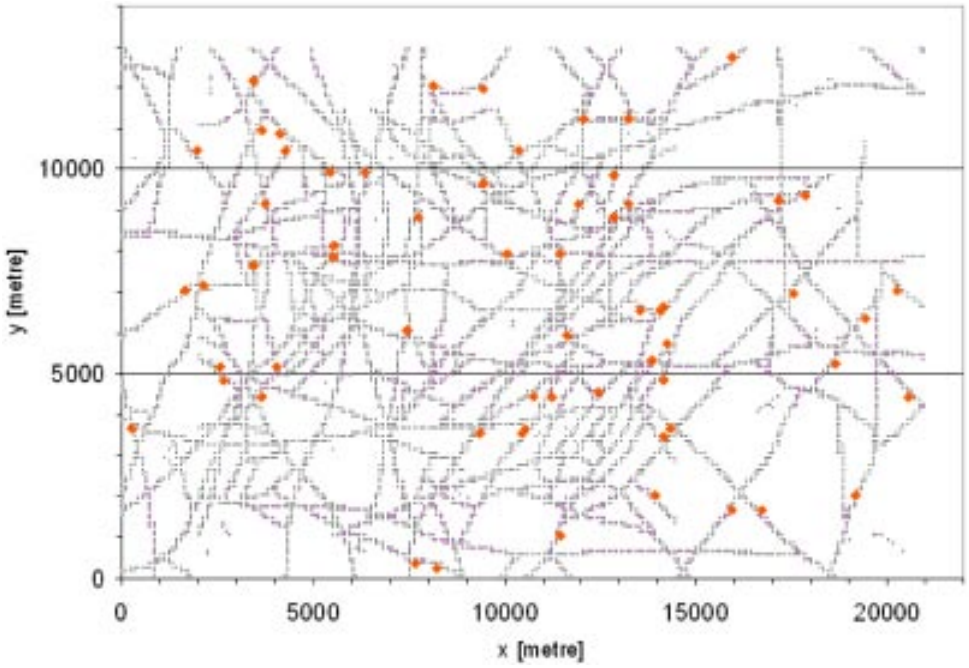

Figure 5-5b. *Illustration of the spatial distribution of the tightest bedrock that experience an increase in salinity early on in the simulation on the elevation –460. The tight bedrock of interest is represented with orange dots and the deterministic deformation zones, (the most permeable parts of the model domain, is represented by the greyish network.*

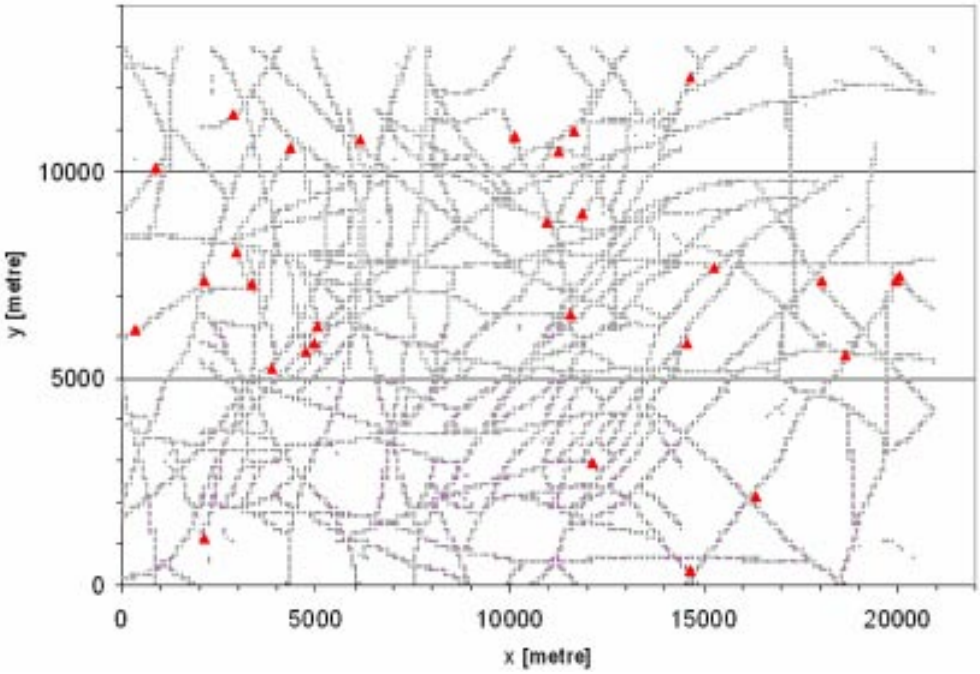

Figure 5-5c. *Illustration of the spatial distribution of the locations that experience the first increase in salinity, data taken from situation after 6 years, on the elevation –460. Locations of interest is represented with the red triangles and the deterministic deformation zones, the most permeable parts of the model domain, is represented by the greyish network.*

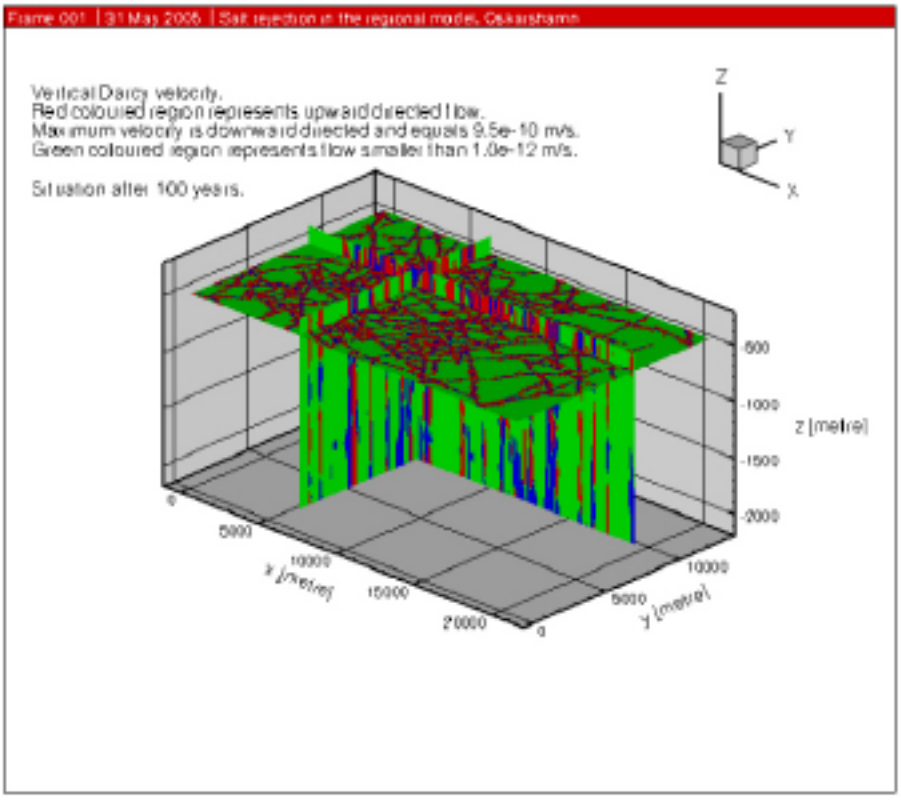

Figure 5-6a. *Distribution of vertical Darcy velocity direction at the depth of 460 m after 100 years. Red colour represents upward flow larger than $1.0 \cdot 10^{-12}$ [m/s], blue colour represents downward flow larger than $1.0 \cdot 10^{-12}$ [m/s]. Green colour represents flow smaller than $1.0 \cdot 10^{-12}$ [m/s] (both upward and downward).*

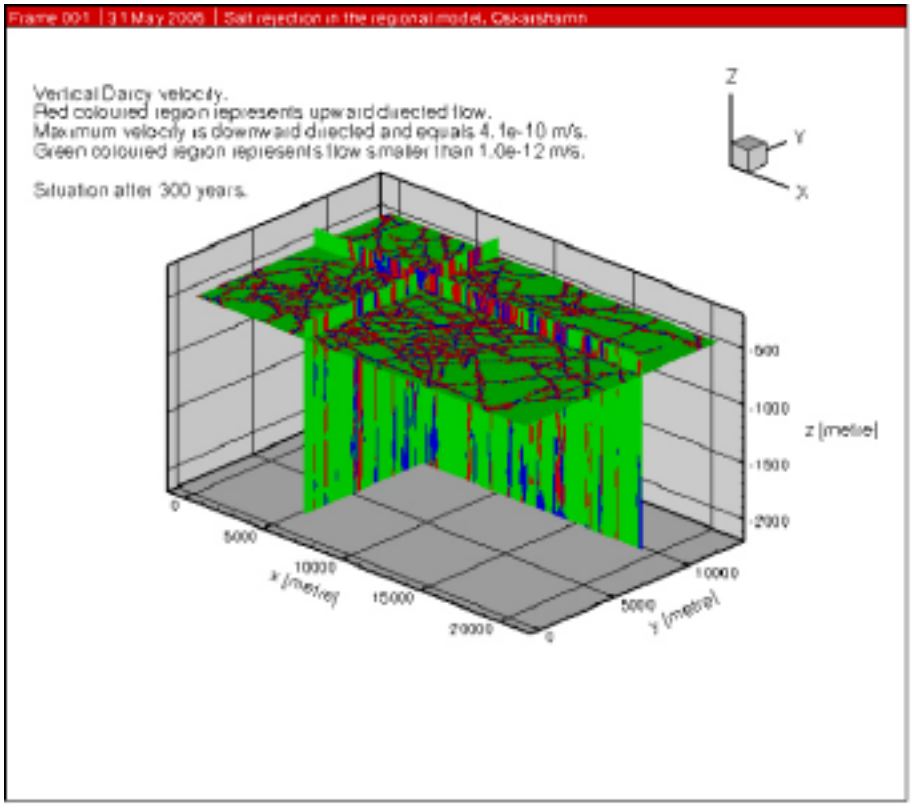

Figure 5-6b. *Distribution of Darcy velocity direction at the depth of 460 m after 300 years.*

Figure 5-7 presents the volume that contains waters from the initial high saline water pulse after 300 years. The figure shows the volume that contains the initial high saline waters released in a uniform layer, after a simulation time of 300 years. It can be seen that most of the initial pulse are still found in the top 800 m and that a large part of the initially released water is still found in its initial location.

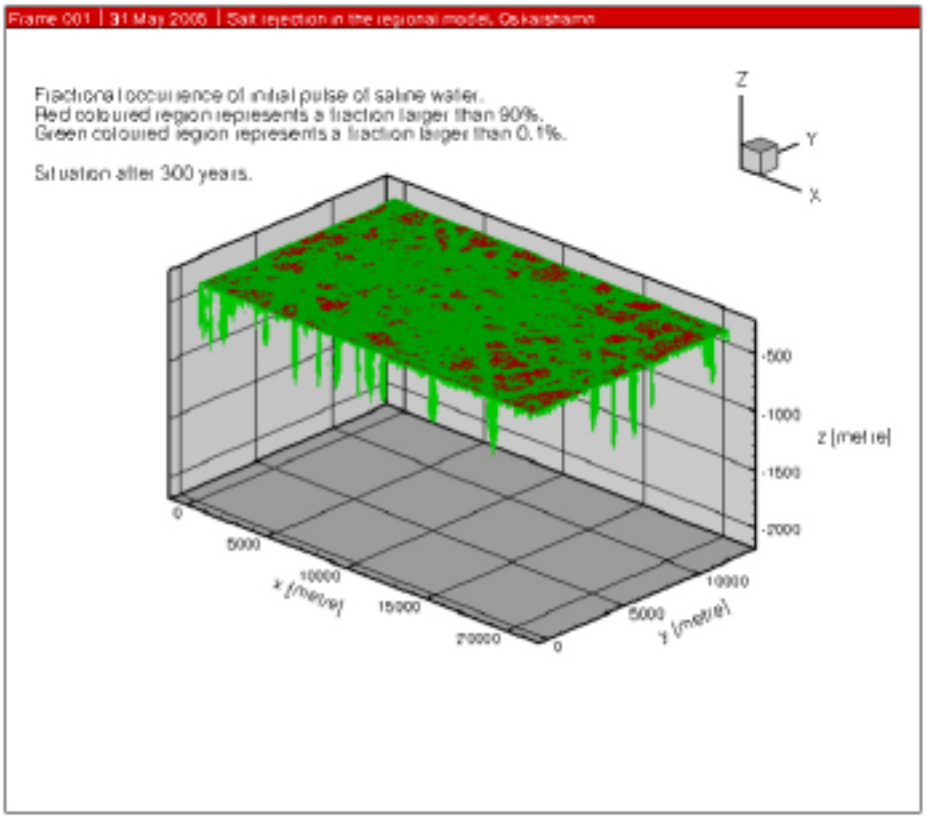

Figure 5-7. *Distribution of the initial pulse of saline waters after 300 years.*

5.1 Sensitivity studies

Figure 5-8a–c illustrate the influence of immobile volumes on the result of the study. The figures show that a larger immobile volume yields larger matrix diffusion and hence less high saline waters are available for downward movement. If the immobile volume is 100 times the mobile volume there are practically no downward movement seen in the first ten years.

Figure 5-9a–b illustrate the situation after 100 years when the bulk permeability values have been decreased 100 times compared to the main simulations. The results of this sensitivity study further support the conclusion that mixing occurs within the more permeable fracture zones. In these sensitivity studies the fracture zones are even more conductive compared to the surrounding bedrock. However, the permeability of the zones is here so low that the high saline waters are practically immobilised within the release layer for the entire simulation time.

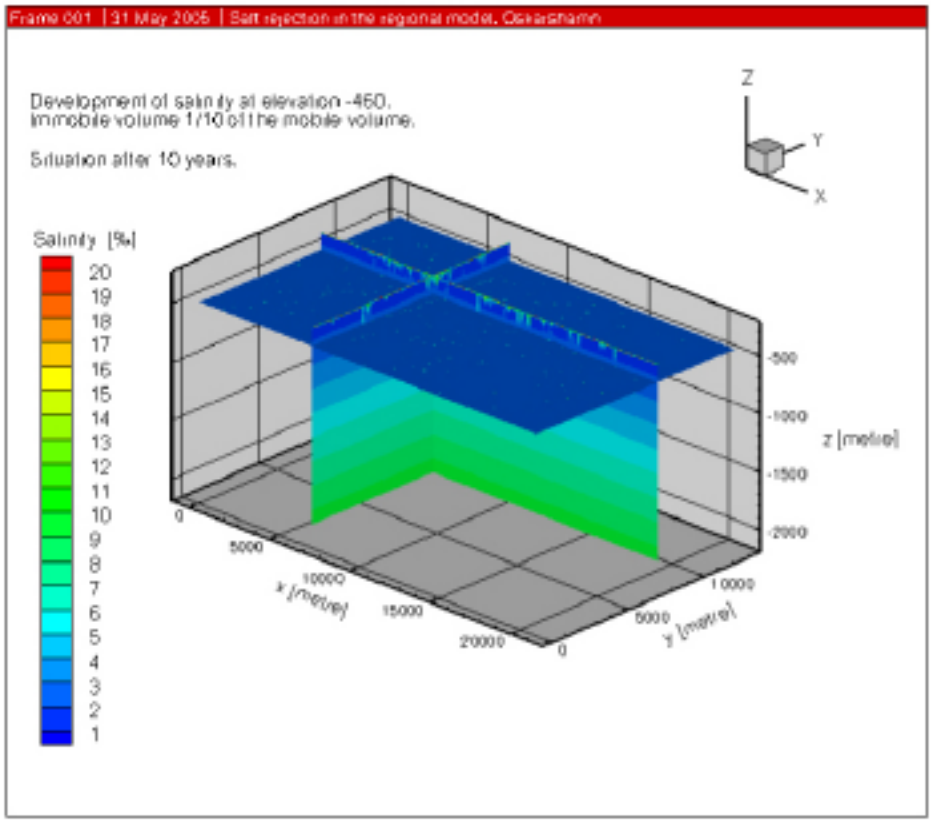

Figure 5-8a. *Effect of the volume available for immobile water (matrix diffusion). The situation after 10 years if the immobile volume is small compared with the mobile volume. The high saline waters move downward and reach a repository depth, approximately 150 m below, within some tens of years.*

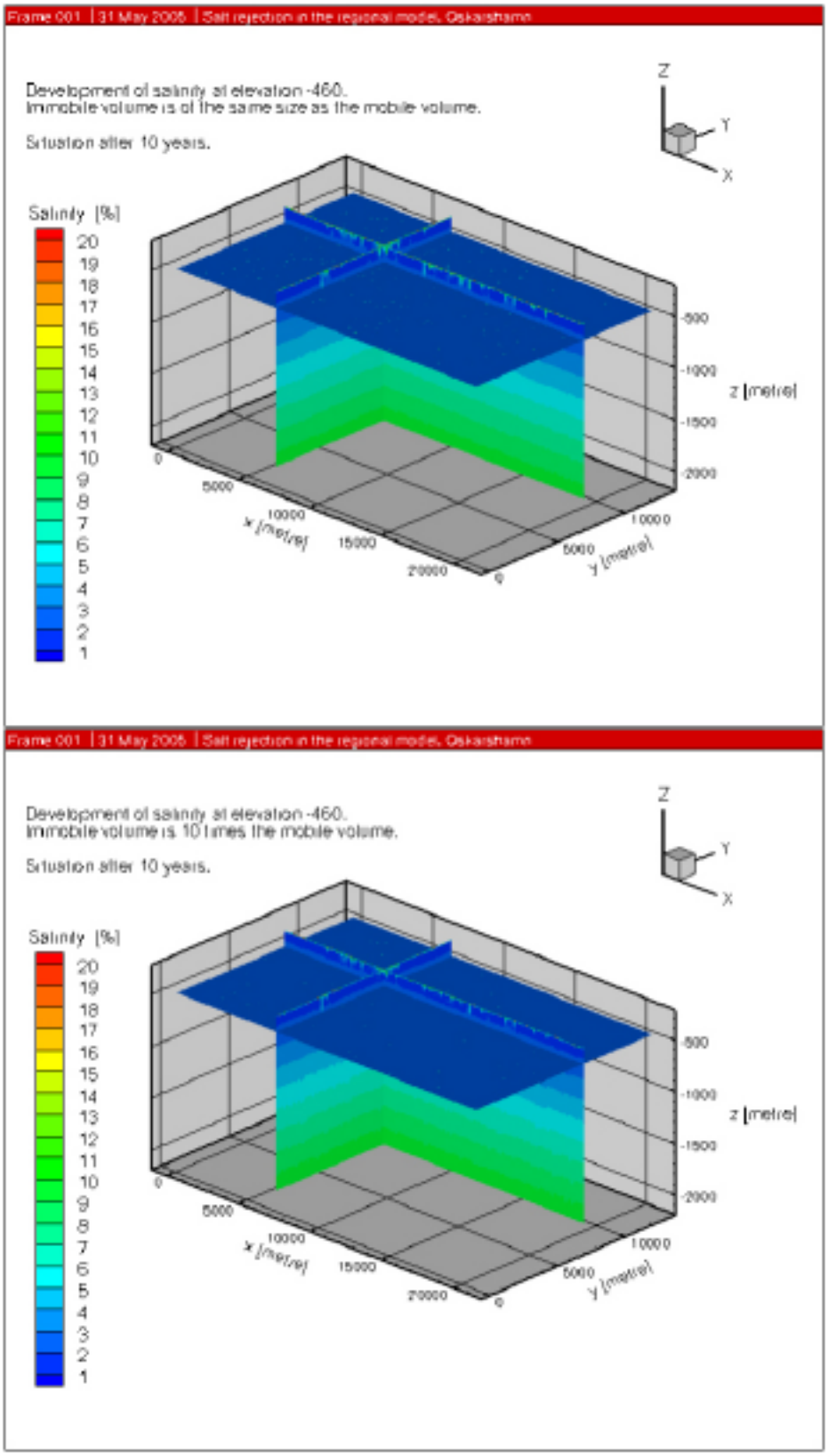

Figure 5-8b. *Effect of the volume available for immobile water (matrix diffusion). Situation after 10 years if the immobile volume is similar (top) or ten times larger (bottom) compared to the mobile volume.*

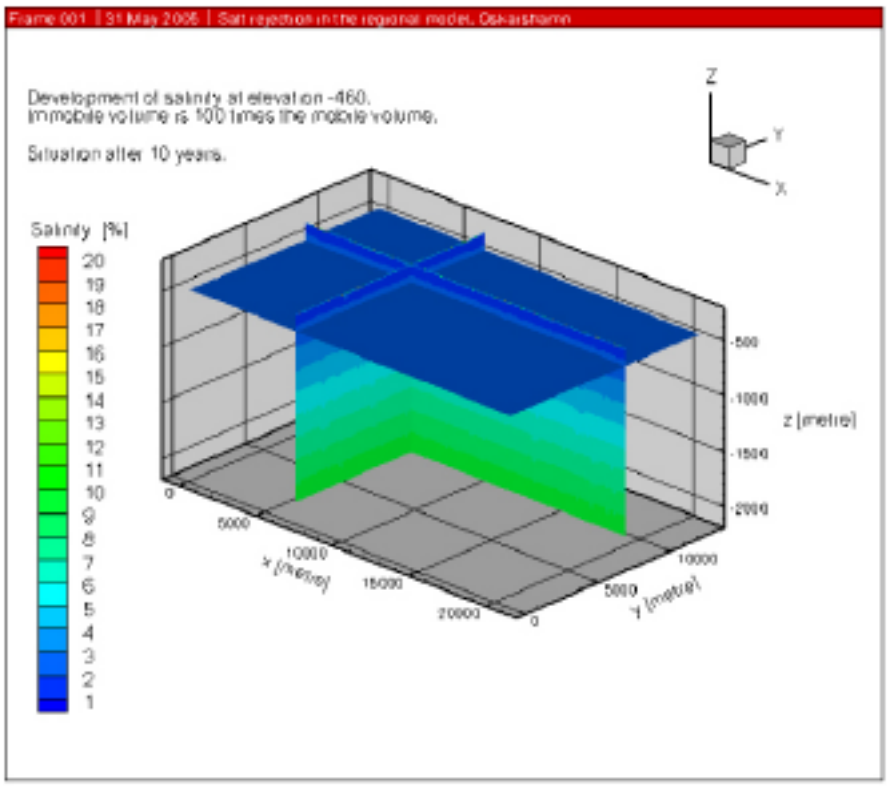

Figure 5-8c. *Effect of the volume available for immobile water (matrix diffusion). The situation after 10 years if the immobile volume is 100 times larger compared with the mobile volume. The high saline waters are practically immobilised at the release level.*

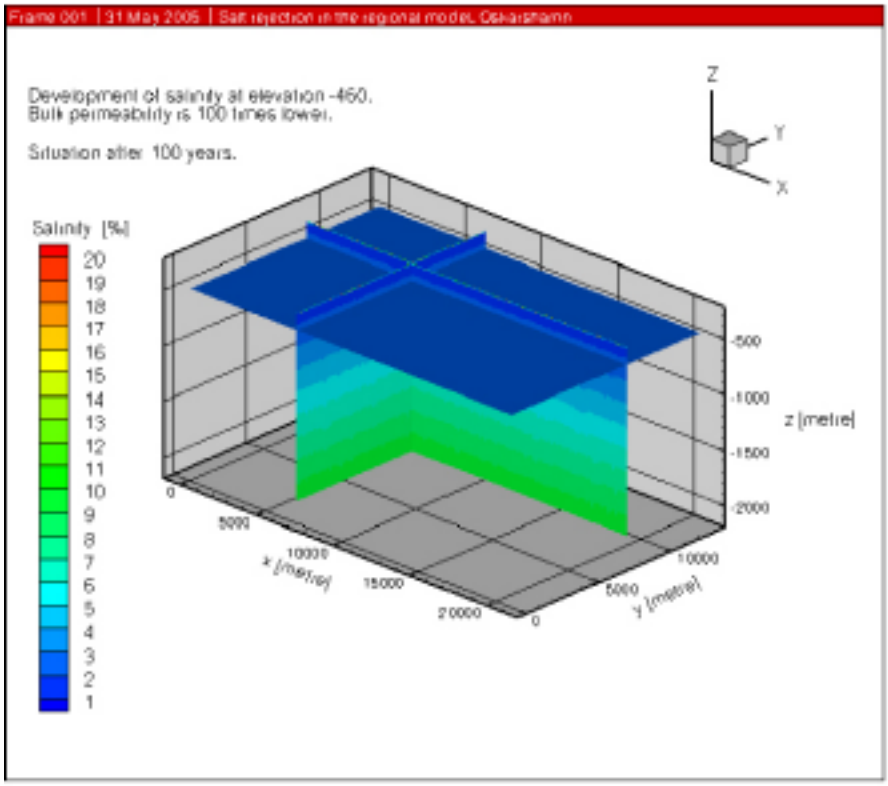

Figure 5-9a. *Effect of a 100 times lower bulk permeability. Situation after 100 years with practically all high saline waters still contained within the release layer.*

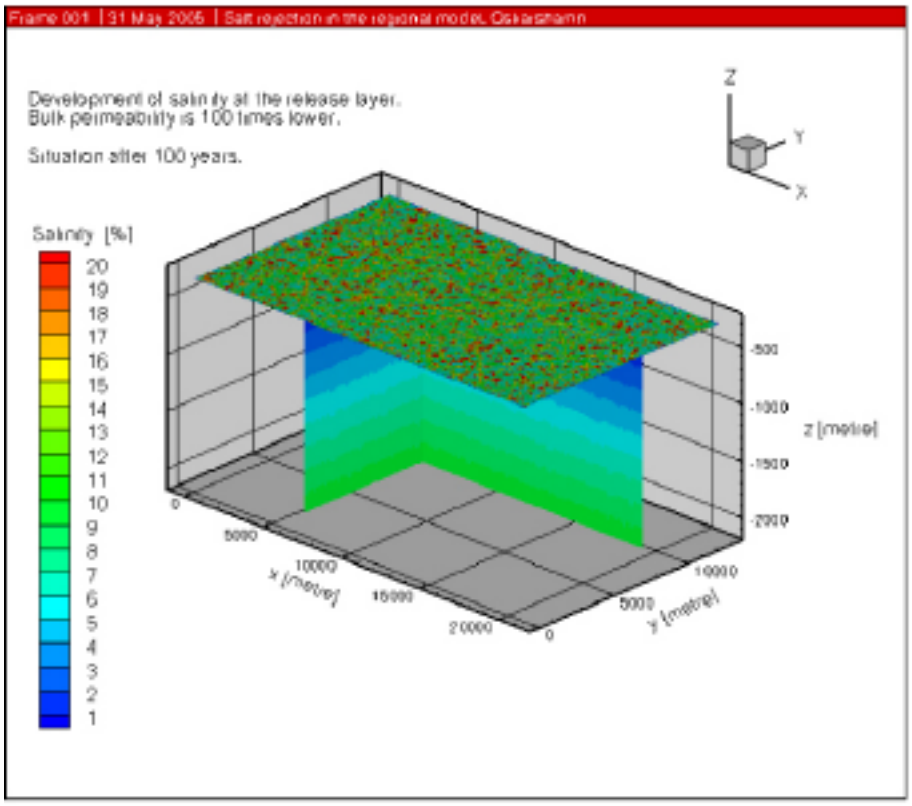

Figure 5-9b. *Effect of a 100 times lower bulk permeability. Surface situation after 100 years.*

6 Discussion and conclusions

In all simulations it is clear that the density-driven mixing occurs within the more permeable network of deterministic deformation zones (the lineament model). The low-permeable surrounding rock mass takes very little part in the density-driven mixing process. Much of the saline water released within such low-permeable regions is still contained within these regions at the end of the simulated time. Figure 5-1 shows the consequence of this. In the figure the low-permeable rock mass still contains saline waters of practically the initial concentration after three-hundred years.

The matrix diffusion affects the salinity within the release layer. However, this effect is highly dependent on the conceptualisation; in our simulation only the mobile water volume is filled with the high saline water and hence a significant volume of immobile water is available for diffusion within this layer. The simulations suggest that much of the diffusion acts on a relatively short time scale and only after some days the low-permeable regions have reached some kind of semi steady-state situation that later on will be little affected by the density-driven mixing.

The vertical Darcy velocities and directions indicate that convection cells primary develop within the deformation zones which are responsible for the majority of the groundwater flux within the model domain.

The salinity distribution over a specific depth elevation, in this case set to –460 m, is found to vary significantly both spatially and temporally. The results indicate that different locations at this depth experience high salinity water at different times after the initiation. This is to be expected due to differences in the hydrogeological properties. Also the matrix diffusion affects the salinity reached at a depth; a larger available immobile volume yields less salinity.

Based on site specific permafrost modelling, the typical permafrost growth rate at Laxemar in the Oskarshamn area, during a glacial cycle, is estimated to be between two and twenty centimetres per year /SKB 2006/. The typical rate of permafrost growth is thus many orders of magnitude smaller than the velocity by which the saline water moves downward within fracture zones as driven by the density difference only. In addition, for fracture zones the porosity values used in the permafrost calculations by /SKB 2006/ are on the lower side compared to porosity values used in our simulations, suggesting even smaller permafrost growth rates.

For the low-permeable bedrock, the time scales for flow and for permafrost growth are either similar or the permafrost growth is faster. As a consequence, it is realistic to assume that a small difference in density at the permafrost interface is not enough to cause a downward groundwater flux in the low-permeable bedrock. Hence, the rejected salt causes an increase in salinity within the local pore volumes and such saline water is assumed to be left as unfrozen saline water inclusions within the permafrost layer. Therefore an initial high salinity pulse would possibly be more realistic if it was contained only within the fracture zones, and not as in this conceptualisation, uniformly over the entire surface. This alternative conceptualisation would not change the salinity values significant since the pore volume – hence salt content – is correlated with the conductive regions. As a consequence of the used conceptualisation the regions just beneath the permafrost containing high saline waters even after the lengthier simulations times should be viewed as conceptual anomalies. It is anticipated that in reality these areas would not be found at a site, but would instead be found as inclusions within the permafrost region.

It has not been investigated how much of the late arrivals of saline waters, possibly indicated by the graphs presented in Figure 5-5a, that are conceptual bias due to the release of saline waters within low-permeable rock mass that continue to “leach” saline waters over significantly longer times (this time scale is significantly longer than the 300 years of the performed simulations).

As mentioned above, analytical calculations of downward Darcy velocities indicate that it is not expected that the saline water originally contained within the permeable deformation zones would take hundreds of years to fall down 160 m. Still, even within the more conductive deformation zones differentiated hydraulic properties are found. Therefore different arrival times are to be expected within a time period of some 10–50 years.

In one of the sensitivity simulations the bulk permeability of the model domain was lowered by two orders of magnitude. In this case the downward flow of saline water disappeared. In fact, no significant change in salinity could be observed 40 m below the permafrost within the simulated one-hundred year period.

Analysing the locations where high salinity waters are found it is clear that many locations at 460 m depth experience saline waters within a couple of years and that the high saline locations successively disappear with time. After approximately 100 years no high saline water (above 5%) is found at 460 m depth. If a correlation analysis between permeability and salinity values is performed it is clear that the majority of high saline waters move down along more conductive regions. However and interestingly, the most conductive regions are not so affected by saline water. Also a salinity "spike" can be observed for the tightest bedrock; these points (locations) are spatially widespread and found primarily within the domain. As illustrated in Figure 5-5b these locations are found in direct contact with the deterministic deformation zones. No further spatial analysis has been performed.

Modelled permafrost growth,such as presented /Hartikainen 2004, SKB 2006/, further suggest that it is realistic to assume that a future permafrost scenario would affect both groundwater recharge and discharge areas and hence that a regional groundwater flow would, at least for a time, cause an effect of flushing the saline water. As seen in the generic case studies a regional groundwater flow is responsible for a "flushing" of saline waters yielding a less saline situation in the sub-surface. The effect of regional flow is not accounted for in the presented results and hence the salinity values are from this aspect a conservative estimate of the values expected at a site.

The no-flow box conceptualisation creates situations of low-pressure in relation to the sinking saline water. This effect of low-pressure is not, however, believed to be a feature that would be observed if in situ field measurements were to be performed. In the real world the permafrost grows in time and it is also plausible that the model domain would contain in- and out-flow regions along with both topographical and larger scale hydraulic gradients.

In summary a few conclusions can be stated:

- The density-driven mixing that occurs beneath a permafrost layer is much faster than modelled site specific permafrost growth rates.
- Generic simulations suggest that a regional groundwater flow beneath a permafrost layer would cause a "flushing" of the rejected salt and hence dilute the salinity at a faster rate than compared with our results.
- The bulk of the mixing process occurs within the more permeable network of deformation zones at a site. For the chosen parameters of these more permeable structures the mixing process acts over 10–50 years. However, the high saline waters practically fall towards the model domain bottom and therefore deeper sections of the more permeable parts of the bedrock experience salinity values up to 9% over this time scale.
- Matrix diffusion is important for the salinity values reached at depth. However, the results are significantly affected by the conceptualisation of the release of salt and also by the available immobile water volume.
- Low-permeable rock mass at a deeper level remains practically unaffected after the simulation time of 300 years.

Based on the findings presented in the present report, a couple of recommendations are suggested:

- Future palaeohydrogeological permafrost scenario simulations ought to incorporate realistic regional flow based on the scenarios simulated. In order to incorporate regional flow it is important to use larger model domains.
- Future palaeohydrogeological permafrost scenario simulations ought to incorporate realistic transient permafrost growth and regions where permafrost will not develop. Again the size of the model domain is important.
- Further tests of the conceptual model concerning issues such as permafrost growth rate, matrix diffusion, and salt rejection are recommended.

References

Darcel C, 2003. Assessment of the feasability of tracer tests with injection in "background fractures" using a model based on a power law fracture length distribution. SKB IPR-03-41. Svensk Kärnbränslehantering AB.

Follin S, Stigsson M, Berglund S, Svensson U, 2004. Variable-density groundwater flow simulations and particle tracking – Numerical modelling using DarcyTools. Preliminary site description of the Simpevarp area – version 1.1. SKB R-04-65. Svensk Kärnbränslehantering AB.

Follin S, Stigsson M, Svensson U, 2006. Hydrogeological DFN modelling using structural and hydraulic data from KLX04. Preliminary site description Laxemar subarea – version 1.2. SKB R-06-24, Svensk Kärnbränslehantering AB.

Haggerty R, Gorelick S M, 1995. Multiple-rate mass transfer for modelling diffusion and surface reactions in media with pore-scale heterogeneity. Water Resources Research 31(10), pp 2383–2400.

Hartikainen J, 2004. Estimation of permafrost depth at Forsmark. TKK-RM-04-05. Helsinki University of Technology. Finland.

Rhén I, Follin S, Hermansson J, 2003. Hydrogeological Site Descriptive Model – a strategy for its development during Site Investigation. SKB R-03-08. Svensk Kärnbränslehantering AB.

Simmons C T, Fenstemaker T R, Sharp Jr. J M, 2001. Variable-density groundwater floe and solute transport in heterogeneous porous media: approaches, resolutions and future challenges. Journal of Contaminant Hydrology 52, pp 245–275.

SKB, 2006. Climate and climate related issues for the safety assessment SR-Can. SKB TR-06-23. Svensk Kärnbränslehantering AB.

Svensson U, 2004. DarcyTools, Version 2.1. Verification and validation. SKB R-04-21. Svensk Kärnbränslehantering AB.

Svensson U, Ferry M, 2004. DarcyTools, Version 2.1. User's guide. SKB R-04-20. Svensk Kärnbränslehantering AB.

Svensson U, Kuylenstierna H-O, Ferry M, 2004. DarcyTools Version 2.1. Concepts, methods, equations and demo simulations. SKB R-04-19. Svensk Kärnbränslehantering AB.

Vidstrand P, 2003. Surface and subsurface conditions in permafrost areas – a literature review. SKB TR-03-06. Svensk Kärnbränslehantering AB.

Vidstrand P, 2004. Internal TN to be incorporated in final report of "Nya Äspömodeller". Modelling reports of Äspö HRL at regional, site, laboratory, and experimental scales.